Impact of 98 LRRK2 variants linked to Parkinson's Disease on kinase activity and microtubule binding

Alexia F Kalogeropulou[1,2*], Elena Purlyte[1,2,6*], Francesca Tonelli[1,2*], Sven M Lange [1], Melanie Wightman [1], Alan R Prescott [3], Shalini Padmanabhan[4,] Esther Sammler [1,5], Dario R Alessi[1,2#]

1. MRC Protein Phosphorylation and Ubiquitylation Unit, School of Life Sciences, University of Dundee, Dow Street, Dundee, United Kingdom.

2. Aligning Science Across Parkinson's (ASAP) Collaborative Research Network, Chevy Chase, MD, USA.

3. Dundee Imaging Facility, School of Life Sciences, University of Dundee, Dundee DD1 5EH, United Kingdom.

4. The Michael J. Fox Foundation for Parkinson's Research, NY, USA.

5. Molecular and Clinical Medicine, Ninewells Hospital and Medical School, University of Dundee, Dundee, DD1 9SY, UK.

6. Current address: Department of Molecular Biology, University of Texas Southwestern Medical Center, Dallas, TX 75390, USA.

* These authors contributed equally to this study.

Corresponding author (d.r.alessi@dundee.ac.uk)

Abstract Mutations enhancing the kinase activity of LRRK2 cause Parkinson's disease (PD) and therapies that reduce LRRK2 kinase activity are being tested in clinical trials. Numerous rare variants of unknown clinical significance have been reported, but how the vast majority impact on LRRK2 function is unknown. Here, we investigate 98 LRRK2 variants linked to PD, including previously described pathogenic mutations, and identify 22 variants that robustly stimulate LRRK2 kinase activity. These include variants within the N-terminal non-catalytic regions [ARM (E334K, A419V), ANK (R767H), LRR (R1067Q, R1325Q)] as well as variants residing within the GTPase domain, predicted to destabilise the ROC:COR_B interface [ROC (A1442P, V1447M), COR_B (S1761R, L1795F)] and COR_B:COR_B dimer interface [COR_B (R1728H/L)]. Most activating variants decrease LRRK2 biomarker site phosphorylation (pSer910/pSer935), consistent with the notion that the active kinase conformation blocks their phosphorylation. We find that the R1628P variant that has been linked to PD does not stimulate LRRK2 activity. We observe that the impact of variants on kinase activity is best evaluated by deploying a cellular assay of LRRK2-dependent Rab10 substrate phosphorylation at Thr73 compared to an *in vitro* kinase assay, as only a minority of activating variants enhance the activity of immunoprecipitated LRRK2, comprising the COR_B (Y1699C, R1728H, S1761R) and kinase (G2019S, I2020T, T2031S) variants. Twelve variants including some that activated LRRK2, suppressed microtubule association in the presence of a Type 1 kinase inhibitor [ARM (M712V), LRR (R1320S), ROC (A1442P, K1468E, S1508R), COR_A (A1589S), COR_B (Y1699C, R1728H/L) and WD40 (R2143M, S2350I, G2385R)]. Our findings will aid in understanding the impact of these variants on LRRK2 kinase activation, stimulate work to reveal mechanisms by which variants impact biology, and provide rationale for variant carrier inclusion or exclusion in ongoing and future LRRK2 clinical trials.

Introduction

1-4% of all cases of PD are caused by genetic changes in Leucine-Rich Repeat Kinase-2 (LRRK2) [1–3]. Additionally, LRRK2 has been linked to modify risk for Crohn's disease (CD) [4]. LRRK2 is a large multidomain enzyme that forms multimeric species [5,6]. It consists of an N-terminus armadillo (ARM), ankyrin (ANK) and leucine-rich repeats (LRR), followed by a C-terminal Roco type GTPase, protein kinase and WD40 domain [7] (Figure 1A). The Roco GTPase domain consists of three subdomains, namely a ROC GTPase followed by two scaffolding domains termed COR_A and COR_B. High resolution Cryo-EM structures of full length [8], as well as the catalytic C-terminal moiety of LRRK2, have been solved in which the catalytic kinase domain is in an inactive open conformation, [9] and more recently in a closed conformation [10]. These structures have provided major insights into the overall structure and function of LRRK2.

LRRK2 is activated following its recruitment to cellular membranes via interactions with Rab29 and other Rab GTPases, likely via its N-terminal ARM domain [11–13]. LRRK2 phosphorylates a subgroup of Rab GTPases at membranes, including Rab8A and Rab10, at a conserved Ser/Thr residue located within the effector binding Switch-II domain [14–16]. This phosphorylation does not impact intrinsic Rab GTPase activity but promotes binding to a new set of effector scaffolding proteins, including RILPL1/2 and JIP3/JIP4 [15,17–20]. Interaction of LRRK2-phosphorylated Rab8A and Rab10 with RILPL1 interferes with ciliogenesis in brain cholinergic neurons in the striatum, decreasing their ability to sense Sonic hedgehog in a neuro-protective circuit that supports dopaminergic neurons [17].

LRRK2-phosphorylated Rab proteins are dephosphorylated by the PPM1H phosphatase [21]. At least in overexpression studies, certain pathogenic mutations, as well as treatment with selective Type I kinase inhibitors that promote the LRRK2 kinase domain to adopt an active conformation, induce helical oligomerization of LRRK2 on microtubule filaments [22–24]. This has been proposed to disrupt vesicle trafficking by causing a "roadblock" for microtubule-based motors [6,9]. The closed, active conformation of LRRK2 also leads to the dephosphorylation of a cluster of phosphorylation sites (Ser910, Ser935, Ser955 and Ser973) located between the Hinge helix and LRR domain through an unknown mechanism [25–27]. Certain pathogenic mutations such as G2019S (located within the kinase domain) promote autophosphorylation of LRRK2 at Ser1292 [28].

Seven missense mutations located within the ROC (N1437H, R1441G/C/H), COR_B (Y1699C), and kinase (G2019S, I2020T) domains have been well-characterized and ascertained to stimulate LRRK2 kinase activity and cause PD [3,29]. The G2019S mutation that substitutes a glycine for serine within the magnesium-binding DYG motif is by far the most frequent PD-associated LRRK2 mutation [30,31]. In addition, a variant located within the WD40 domain (G2385R), is common in Chinese Han and Taiwanese populations and moderately increases PD risk; biochemical analysis suggests that G2385R blocks WD40 dimerization and moderately enhances LRRK2 kinase activity [32–34]. Over 1000 rare variants of LRRK2 have been reported [35–37], and a recent study employed a computational tool that reportedly predicts a Parkinson's pathogenic "REVEL score" for each variant, with a score > 0.600 predicted to be pathogenic [38–40].

Here we describe a robust workflow to experimentally evaluate LRRK2 variant impact on LRRK2 function. Specifically, we utilize LRRK2-dependent Rab10 phosphorylation at Thr73 as a readout for the LRRK2 kinase pathway activity ($pRab10^{Thr73}$), using selective phospho-specific antibodies [41]. From amongst 98 LRRK2 variants, we identified 22 that robustly enhance LRRK2 kinase activity, defined as >1.5-fold above LRRK2 wildtype. These include novel variants within the N-terminal, non-catalytic ARM, ANK and LRR regions, as well as within the COR_B and ROC domain, that are predicted to destabilise the interface between the ROC and COR_B domain or impact the COR_B:COR_B dimer interface. Amongst the 98 variants tested, we also report a subset of 12 variants that suppress the ability of LRRK2 to bind microtubules in the presence of Type 1 LRRK2 kinase inhibitors. Overall, our work will assist in the interpretation of the many reported LRRK2 variants of unknown clinical significance identified in individuals and families with PD [38], by informing on variant impact on LRRK2 function and providing a framework for the thorough functional characterization and cataloguing of other LRRK2 variants of unknown significance. In fact, the functional stratification of LRRK2 variants is particularly important in view of targeted treatments such as LRRK2 kinase inhibitors entering clinical trials.

Results

Selection of LRRK2 variants

98 LRRK2 variants were selected from previous genetic analysis of PD patients (STable 1). This list includes the 7 "definitely pathogenic" mutations as listed in the MDSgene database (https://www.mdsgene.org) [ROC (N1437H, R1441 hotspot mutations), COR_B (Y1699C),

KINASE (G2019S, I2020T)] as well as 4 previously characterized variants, including the KINASE (T2031S, N2081D) and WD40 (G2385R) variants that activate LRRK2 (Fig 1A). Variants linked to increased CD disease risk [ARM (N551K) and KINASE (N2081D)] as well as a variant reported to protect from PD and CD [ROC (R1398H)] were also included [4]. Other than the well characterized variants mentioned above, the remainder have only been reported in a single or small number of cases and studies and often without clear evidence of pathogenicity in line with current guidelines [42]. Literature citations and REVEL scores [38] (http://database.liulab.science/dbNSFP) for each of the selected variants, as well as evolutionary conservation scores for each variant amino acid determined using the Consurf database (https://consurf.tau.ac.il/) [43], are tabulated in STable 1. The selected variants are located within the following domains: ARM (18), ANK (9), LRR (12), ROC (15), COR_A (6), COR_B (8), kinase (9) and WD40 (14) domains, as well as between the boundaries of the ANK and LRR (5), and LRR and ROC domains (2) (Fig 1A).

Impact of variants on LRRK2 activity in a cellular assay

To assess the impact of each variant, we utilised a HEK293 cell overexpression system (summarized in Figure 1B) and assessed LRRK2-mediated pRab10^{Thr73}, LRRK2 autophosphorylation at Ser1292, as well as LRRK2 biomarker site phosphorylation (Ser935, Ser955 and Ser973). HEK293 cells lend themselves for the interrogation of LRRK2-dependent pRab10^{Thr73} phosphorylation as they have low levels of endogenous LRRK2 but high endogenous Rab10 expression with resulting complete lack of phosphorylation at the LRRK2-dependent Rab10^{Thr73} phospho-site. In a primary screen, all 98 variants were analysed in parallel and normalized to the effect of the LRRK2 wildtype protein, and data were merged from up to 6 independent screens (Fig 1C, 2, SFig 1, SFig 2). LRRK2 variant impact on LRRK2 kinase activity was defined as 'activating' if pRab10 ^{Thr73} levels were >1.5-fold and 'reduced' if pRab10 ^{Thr73} levels were <0.5-fold relative to the LRRK2 wildtype protein. Our analysis highlighted 23 variants [ARM (E334K, A419V), ANK (R767H), LRR (R981K, R1067Q), boundary between LRR and ROC (R1325Q), ROC (**N1437H**, **R1441G/C/H/S**, A1442P, V1447M), COR_B (**Y1699C**, R1728H/L, S1761R, L1795F), kinase (**G2019S**, **I2020T**, **T2031S**, **N2081D**) and WD40 (**G2385R**)], that activate LRRK2 kinase activity (Fig 1C, SFig 1). Eleven of these variants (shown in bold) had previously been reported to stimulate LRRK2 kinase activity. Using the same overexpression system, we then reanalysed all 23 activating variants from the primary screen in a secondary quantitative immunoblot analysis, in which we confirmed 22 of the 23 variants to robustly enhance LRRK2-mediated Rab10^{Thr73} phosphorylation >1.5-fold above wildtype (Fig 3). Only the LRR R981K variant fell below the 1.5-fold cut-off and could not be confirmed to be activating in the secondary assay (Fig 3). It should be noted that the R1628P variant that has been linked to PD in numerous studies [36,44], had no impact on LRRK2 kinase activity (Fig 1C, SFig 1). Thus, from the group of 98 LRRK2 variants analysed, 22 activated, 74 had no effect and 2 variants [ROC (S1508R) and COR_A (A1589S)] significantly reduced LRRK2 kinase activity.

The G2019S mutation stimulated LRRK2 Ser1292 autophosphorylation ~10-fold, to a greater extent than other variants (Fig 2A, Fig 3A, D, SFig 1). Nine variants [ROC (N1437H, R1441G/C/S/H, A1442P) and COR_B (Y1699C, S1761R, L1795F)], increased Ser1292 autophosphorylation 2- to 4-fold (Fig 2A, Fig 3A, D, SFig 1). Previous work revealed that variants that activate LRRK2 kinase activity such as ROC (R1441G/C) and COR_B (Y1699C) suppressed LRRK2 biomarker phosphorylation, likely by promoting the closed, active

conformation of the LRRK2 kinase domain [25–27]. Consistent with this, 10 activating variants [ROC (N1347H, R1441G/H/S, A1442P, V1447M), COR_B (Y1699C, L1795F), kinase (I2020T) and WD40 (G2385R)], displayed >2-fold reduction in phosphorylation of all biomarker sites (Fig 2B, Fig 3A, E, SFig 1). Seven variants [(ARM (E334K and A419V), LRR (R1067Q), ROC (R1441C) and COR_B (R1728H/L and S1761R)] showed reduced Ser955 phosphorylation, with moderate impact on Ser935 and Ser973 phosphorylation (Fig 2B, Fig 3A, E, SFig 1, SFig 2). The reduced activity variants [ROC (S1508R) and COR_A (A1589S)], possessed similar biomarker phosphorylation as wildtype LRRK2 (Fig 2B, Fig 3A, E, SFig 1, SFig 2). Two variants [ARM (I388T) and ANK (M712V)] decreased biomarker site phosphorylation without impacting LRRK2-dependent $Rab10^{Thr73}$ phosphorylation (Fig 1C, Fig 2B, Fig 3A, E, SFig 1, SFig 2). None of the variants studied increased the basal level of phosphorylation of the biomarker sites. The R1398H protective variant [45] displayed similar $pRab10^{Thr73}$, pSer1292 and LRRK2 biomarker phosphorylation in our analysis compared to that of wildtype LRRK2 (Fig 1C, SFig 1, SFig 2). None of the variants analysed markedly impacted LRRK2 expression levels in HEK293 cells (Fig 2C, Fig 3B, SFig 1).

Impact of variants in an immunoprecipitation *in vitro* assay

Previous work revealed that pathogenic LRRK2 variants, such as the common G2019S kinase domain variant, directly enhance LRRK2 kinase activity, and this effect was recapitulated in recombinant *in vitro* kinase assays [46,47]. In contrast, other pathogenic variants, such as ROC (R1441G), despite enhancing LRRK2 kinase pathway activity to a greater extent than the G2019S variant *in vivo*, failed to stimulate kinase activity of recombinant LRRK2 *in vitro* [47]. The contrasting effects on *in vitro* kinase activity suggest that these variants activate LRRK2 in cells by a different mechanism. This prompted us to investigate which of the *in vivo* activating variants enhanced activity of recombinant LRRK2 in an *in vitro* kinase assay. We expressed and immunopurified FLAG-tagged wildtype or mutant LRRK2 in HEK293 cells and subjected the purified protein to an *in vitro* kinase assay employing recombinant Rab8A as a substrate (Fig 4A). LRRK2-mediated phosphorylation of Rab8A at Thr72 was quantified using a previously characterized pan-selective phospho-Rab antibody [41](Fig 4A). We observed that from the 22 variants found to enhance LRRK2 kinase activity as measured by $pRab10^{Thr73}$ in the cellular assay, only 7 enhanced Rab8A phosphorylation *in vitro* immunoprecipitation kinase activity by >1.5-fold [COR_B (Y1699C, R1728H, R1728L, S1761R) and kinase (G2019S, I2020T and T2031S)] (Fig 4B, SFig 3, SFig 4). The kinase G2019S variant enhanced *in vitro* Rab8A phosphorylation around 3-fold with the COR_B Y1699C and kinase T2031S variants stimulating activity ~4-fold (Fig 4B, SFig 3, SFig 4). None of the variants within the ARM, ANK, LRR, ROC or WD40 domains enhanced immunoprecipitated LRRK2 activity *in vitro* (Fig 4B, SFig 3, SFig 4). The variants displaying reduced activity in the cellular assay [ROC (S1508R) and COR_A (A1589S)] possessed similar *in vitro* kinase activity towards Rab8A as the immunoprecipitated wildtype LRRK2 (Fig 4B, SFig3, SFig 4), suggesting that these may impact LRRK2 kinase pathway activity in cells by an indirect mechanism rather than having a direct effect on LRRK2 kinase activity. Four variants [COR_B (Y1699C, R1728H) and kinase (G2019S, T2031S)] enhanced Ser1292 autophosphorylation over 2-fold in an *in vitro* assay (Fig 4C, SFig 3, SFig 4). We also studied autophosphorylation of LRRK2 at Thr1357 [48] and Thr1503 [49] employing recently developed phospho-antibodies. This revealed that the COR_B (R1728H) as well as the 3 kinase variants (G2019S, I2020T and T2031S) enhanced

autophosphorylation of these sites ~2- to 4-fold (Fig 4D, SFig 3, SFig 4). Since both COR_B and kinase domain variants increase LRRK2 activity in an immunoprecipitation assay, we next explored the impact of combining COR_B and KINASE domain activating variants on LRRK2 kinase activity *in vitro*. This revealed that the Y1699C+T2031S as well as the Y1699C+G2019S combination increased LRRK2-mediated Rab8A phosphorylation to a greater degree than individual mutations assayed in parallel experiments (Fig 4E, SFig 5). The Y1699C+G2019S combination also increased Ser1292 autophosphorylation *in vitro*, ~12-fold, to a significantly greater extent than any other combination of mutations tested (Fig 4E, SFig 5).

Activation of variants by overexpression of Rab29

Overexpression of Rab29 recruits LRRK2 to the Golgi membrane, promoting stimulation of LRRK2 kinase activity as assessed by increased $Rab10^{Thr73}$ phosphorylation and LRRK2 Ser1292 autophosphorylation [11,12,50]. We next studied the impact of Rab29 overexpression on the activating variants and observed enhanced $Rab10^{Thr73}$ phosphorylation and Ser1292 autophosphorylation with all variants tested (Fig 5, SFig 6). All ROC:COR_B domain interface variants enhanced Ser1292 autophosphorylation to a higher extent than the COR_B:COR_B interface variant (R1728H/L) following overexpression of Rab29 (Fig 5B, SFig 6). Rab29 also increases the activity of the two variants displaying reduced activity [ROC (S1508R) and COR_A (A1589S)] (Fig 5A). Co-expression of Rab29 decreased LRRK2 Ser935 phosphorylation of all variants (Fig 5C). All variants phosphorylated Rab29 as a substrate at Thr71 to a similar extent (SFig 6), consistent with these being similarly activated by Rab29 binding.

Impact of variants on MLi-2 induced microtubule association

As mentioned in the introduction, Type 1 LRRK2 inhibitors including MLi-2, promote ordered oligomerization of LRRK2 on filaments [22–24]. We next investigated how the selected 98 LRRK2 variants impacted MLi-2 induced microtubule association. Cells expressing wildtype or LRRK2 variants were treated ± 100 nM MLi-2 for 3 hours, prior to fixation with 4% (w/v) paraformaldehyde. Immunofluorescence analysis was performed blinded and the fraction of cells displaying filamentous LRRK2 was quantified by studying 50-221 LRRK2 signal-positive cells in two separate experiments (Fig 6). In the absence of MLi-2, typically <5% cells of wildtype LRRK2 and most of the variants displayed filamentous LRRK2. For a few variants [ARM (G393V, A419V), ROC (N1437H) COR_B (R1725Q), KINASE (I2020T) and WD40 (T2494I)], moderately elevated filamentous LRRK2 was observed in the absence of MLi-2. Consistent with previous work, MLi-2 treatment markedly increased the proportion of cells displaying filamentous LRRK2 to above 20 % for wildtype and the majority of studied variants. On the contrary, the kinase inactive LRRK2[D2017A], displayed no significant increase in filament formation following MLi-2 administration. In addition, we observed that microtubule association in the presence of a Type 1 inhibitor was substantially reduced to below <10% of cells for 12 variants [ARM (M712V), LRR (R1320S), ROC (A1442P, K1468E, S1508R), COR_A (A1589S), COR_B (Y1699C, R1728H/L) and WD40 (R2143M, S2350I, G2385R)]. We also observed that a further 13 variants [ANK (P755L, T776M, R793M), LRR (S1228T), ROC (R1398H, R1441S, V1447M), COR_A (P1542S, R1628P), KIN (R1941H) and WD40 (T2141M, D2175H, Y2189C)] displayed a moderate reduction in MLi-2 induced microtubule association.

Discussion

In this study, we employed a tried and tested workflow to assess the activity of 98 LRRK2 variants that have previously been linked in the literature to PD (STable 1). The data obtained with respect to how each variant impacts pRab10^{Thr73}, pSer935, pSer1292 phosphorylation is summarized in Figure 7A. Most importantly, we have characterised a group of 22 variants that reproducibly and robustly stimulate LRRK2-mediated Rab10^{Thr73} substrate phosphorylation >1.5-fold in the HEK293 cell overexpression system (Fig 1 to 3). We investigated how the pathogenic REVEL score [38] of each variant (STable 1) correlates with experimentally measured variant activity and observed that 13 of the 22 activating variants possessed a REVEL score of > 0.6, which is considered pathogenic (Fig 7C). These included most of the previously characterised pathogenic mutations, as well as some of the novel variants identified in this study [ROC (A1442P, V1447M), COR$_B$ (L1795F, R1728H/L)]. The activating variants located outside of the catalytic domains [ARM (E334K, A419V), ANK (R767H), LRR (R1067Q, R1325Q), COR$_B$ (S1761R)] displayed REVEL scores of < 0.6 (Fig 7B). Only one of the variants tested, I2012T, possessed a REVEL score > 0.6 and did not stimulate LRRK2 in our assays (Fig 7B). Thus, 72 of the 73 variants studied, that did not enhance LRRK2 activity, displayed a REVEL score of < 0.6 (Fig 7B). We next explored how the evolutionary conservation score of each variant residue (STable 1) correlates with cellular kinase activity (Fig 7C). For this analysis, the evolutionary conservation was calculated using the ConSurf Server [43] and given a score of 1 to 9, with 1 being the least conserved, 4 with average conservation and 9 being the most conserved. Functionally important residues that control kinase activity would be expected to be highly evolutionarily conserved. Consistent with this, 20 of the 22 LRRK2 activating variants possess a high evolutionary conservation score of 7 to 9 (Fig 8C). Only two activating variants, namely E334K (score 6) and G2385R (score 5), possess a lower score. Interestingly, the LRR R981K variant that was selected for our secondary screen and found not to significantly increase LRRK2 activity (Fig 3), possesses a low REVEL (0.062) and conservation score (3), consistent with these parameters being useful for assessing pathogenicity. The R1628P variant that has been linked to PD in numerous studies [36,44], which had no impact on LRRK2 kinase activity (Fig 1C, SFig 1) possesses a high conservation score of 8 and a REVEL score of 0.54. The high conservation score of this residue is indicative of an important functional role and further work is needed to understand how the R1628P variant impacts LRRK2.

Our data suggest that the impact of variants on LRRK2 kinase activity, is better assessed employing a cellular assay measuring LRRK2-dependent pRab10^{Thr73} levels (Fig 1 to 3), rather than in an immunoprecipitation *in vitro* kinase assay (Fig 4), as only 7 of the 22 variants that enhanced activity in the cellular assay stimulated kinase activity *in vitro* [COR$_B$ (Y1699C, R1728H, R1728L, S1761R) and kinase (G2019S, I2020T and T2031S)]. It is likely that the mutants that activate LRRK2 in the *in vitro* assay, stabilize the active conformation of the kinase domain. Further work is required to understand the mechanism by which most of the other identified variants stimulate LRRK2 kinase activity in cells. It is possible that these variants facilitate membrane interaction and/or association with other factors that enhance LRRK2-mediated phosphorylation of Rab10^{Thr73}. We also observed that combinations of Y1699C with G2019S or T2031S stimulated *in vitro* LRRK2 kinase activity to a greater extent

than each individual variant alone (Fig 4E) and this finding may be useful in generating highly active LRRK2 constructs for future functional and/or structural analysis.

The 22 identified activating variants are located across all domains of LRRK2 apart from the COR_A, Hinge-helix and C-terminal helix (Fig 3A). Utilizing available high-resolution structures of inactive full-length LRRK2 and LRRK2 WD40 domain dimer (Protein Data Bank (PDB) 7LI4, 7LHT [8], PDB 6DLO [33]), and the LRRK2 model from the EMBL-EBI AlphaFold database (AFDB) [51] (Fig 8A, B, C), we have analysed how these variants may impact LRRK2 structure and function. Three activating variants (G2019S, I2020T and T2031S) locate to the kinase active site (Fig 8D). Previous structural studies and molecular dynamics analyses of the G2019S and I2020T mutants suggest that they activate LRRK2 through changes in the flexibility of the kinase activation segment [8,52–54]. The T2031S variant is also located in the activation segment and may have a similar mechanism of kinase activation as G2019S and I2020T. An intriguing common feature of most of the other activating variants is that they appear to destabilise LRRK2 interdomain interfaces outside of the kinase domain. Most of these activating LRRK2 variants locate to the ROC and COR_B domains and lie within or nearby to the ROC:COR_B interface. These residues either participate in the interaction of the two domains directly [ROC (N1437H, R1441G/C/H/S), COR_B (Y1699C, L1795F)] or stabilize elements of the interface indirectly [ROC (A1442P, V1447M), COR_B (S1761R)] (Fig 8E). In addition, the COR_B variants R1728H/L locate to the COR_B:COR_B dimer interface of LRRK2 (PDB 7LHT, Fig 8F). While the R1728 side chain is not fully resolved in the LRRK2 dimer structure, it is likely to form hydrogen bonds with the carbonyl backbone of P1683 and L1682, as well as the side chain of E1681 (Fig 8F). The activating variants in the ROC and COR_B domains are therefore predicted to destabilize the ROC:COR_B and COR:COR interfaces. Further, the R767H variant likely destabilises the ANK:C-terminal helix interface, as the arginine side chain of the R767 bridges the ANK domain to the C-terminal helix through hydrophobic and polar interactions with V2513 and E2516, respectively (Fig 8G). The LRR variant R1067Q variant may disrupt the LRR:kinase interface, as R1067 interacts with the kinase N-lobe through polar interactions with the carbonyl-backbone of F1883 (Fig 8H). The CD-associated N2081D variant is also found in the LRR:kinase interface and forms a hydrophilic interaction with residues of the LRR domain (Fig 8I), and this mutation has been proposed to disrupt these interactions [8]. The R1325Q variant resides at the LRR:COR_A interface, where the aliphatic part of the arginine side chain is involved in hydrophobic contacts with F1321 and P1524, while the guanidinium group is engaged with N1286 via polar interactions (Fig 8J). The common G2385R risk factor variant maps to the WD40:WD40 dimer interface, and mutation of this residue to arginine is likely to cause steric clashes with the neighbouring LRRK2 molecule and has been reported to block dimerization of this domain ([33], Fig 8K). Noteworthy, the G2385R variant may also exert its pathogenic effect through coulomb repulsion with R841 of the Hinge-helix as previously proposed [8]. Finally, two of the identified activating variants, E334K and A419V, map to the N-terminal region of the ARM domain, which is absent from currently available high-resolution structures. However, the AlphaFold model of this region in LRRK2 (residues 159-511) has high local confidence scores (pLDDT) and agrees well with the experimentally determined cryo-EM map of LRRK2 (AFDB Q5S007-F1, EMD-23352,[8])(SFig 7). In the AlphaFold model, E334

locates to an unstructured loop (residues 328-347) that protrudes from the armadillo repeats region (Fig 8L). Interestingly, this loop is highly acidic with 11 Asp/Glu out of 20 total residues and charge reversal through the E334K variant may therefore change the nature and function of this acidic loop. In contrast, the second ARM variant A419V is buried in the armadillo repeats and not solvent exposed, and mutation to Val is likely to disturb the ARM structure (Fig 8L). Together, the activating ARM variants point to a third mechanism in regulating LRRK2 kinase activity, not yet explained by existing structures. We speculate that these mutations may affect substrate access, as the N-terminal ARM has previously been implicated in Rab substrate binding [13].

We also identify 12 variants [ARM (M712V), LRR (1320S), ROC (A1442P, K1468E, S1508R), COR_A (A1589S), COR_B (Y1699C, R1728H/L) and WD40 (R2143M, S2350I, G2385R)], in addition to kinase inactive LRRK2[D2017A], that significantly suppressed microtubule association in the presence of the MLi-2 Type 1 LRRK2 kinase inhibitor (Fig 6). Previous studies have established that the ROC-COR-kinase-WD40 domain fragment is sufficient to mediate oligomerization onto microtubules [9], and revealed that mutations impacting the WD40:WD40 interface [22] or the COR_B:COR_B interface [8], block microtubule association in cells. These conclusions are confirmed by a recent study that also highlights that disrupting the COR_B:COR_B interface by introducing the R1731L/D mutation, or the WD40:WD40 interface by introducing the S2343D mutation, markedly blocks microtubule association [10]. These findings likely account for why we observed that the COR_B (R1728H/R1728L), as well as the WD40 (R2143M, S2350I, G2385R) variants that likely effect the COR_B:COR_B and WD40:WD40 interfaces, inhibit microtubule association. Recent analysis identified a set of key basic residues located within the ROC domain that directly interact with acidic microtubule residues and this interaction is disrupted by a ROC (R1501W) variant linked to PD [10]. The ROC S1508R variant that we identified to block microtubule association is an internally buried residue in the ROC domain that is located adjacent to the basic microtubule-interacting patch and could affect positioning of the basic microtubule-binding patch. K1468E is on the ROC domain surface pointing towards the microtubule surface. This residue is not part of the characterised microtubule-binding basic patch but located nearby and could also participate in microtubule binding. If the kinase inactivating D2017A variant impacts MLi-2 binding, this would account for why this mutation blocks MLi-2 mediated microtubule association. The mechanism by which ARM (M712V), LRR (R1320S), ROC (A1442P) and COR_B (Y1699C) variants interfere with microtubule binding is currently not clear and requires further investigation.

It has been suggested that the ability of pathogenic variants to associate with microtubules may be linked to Parkinson's disease [9]. The finding that 7 activating variants [ROC (A1442P), COR_B (Y1699C, R1728H/L) and WD40 (R2143M, S2350I, G2385R)] displayed reduced microtubule association, highlights that further analysis is required to explore a potential link between microtubule binding and PD. Interestingly, a recent study characterizing the R1731L and R1731D mutations that interfere with the COR_B:COR_B dimer interface, also observed that these mutations enhanced LRRK2 kinase activity [10], similar to

what we have observed with the R1728H/L variants. The mechanism by which disruption of the COR_B:COR_B interface promotes kinase activation is currently unknown.

LRRK2 is a large protein with 2527 residues, and over 1000 variants have been reported and cumulatively many people with PD patients likely carry rare LRRK2 variants of unknown clinical significance [38]. With next generation sequencing becoming more readily available for people with PD and disease modification with targeted treatments including LRRK2 kinase inhibitors entering clinical trials, , there is increased urgency to have a concrete set of functional parameters and experimental workflows to help clinicians assess whether any given LRRK2 variant is likely to increase kinase activity and therefore a likely driver of disease. We advocate the use of the experimental HEK293 cellular assay (Fig 1 to 3) to assess whether a variant activates LRRK2 kinase activity by measuring LRRK2-dependent $Rab10^{Thr73}$ phosphorylation, rather than the *in vitro* kinase assay (Fig 4) or solely relying on predictive methodology. Although the REVEL pathogenic score is useful, our data highlight that the REVEL score fails to identify most activating variants lying outside the GTPase and kinase domains (Fig 7B). A conservation evolutionary score of 7 to 9 would also indicate that the variant lies within a functionally critical position of the protein and most activating variants displayed conservation scores within this range. In future work, we are planning to experimentally assess additional LRRK2 variants linked to PD as they are reported. We are aiming to deposit all experimental data, REVEL and evolutionary conservation scores into a publicly accessible database (e.g., in collaboration with the Movement Disorder Society Genetic mutation database (MDSGene)) as soon as data becomes available. We hope that this information will help clinicians interpret LRRK2 variants in terms of their pathogenicity for genetic counselling, stratify people with LRRK2 variants and make a case to prioritize these individuals for LRRK2-targeting clinical trials, as well as stimulate further mechanistic and structural analysis to better understand how these variants enhance LRRK2 kinase activity. There is also a need to validate similar functional workflows for other PD-associated genes, including the lysosomal enzyme glucocerebrosidase (GBA) [57].

Materials and Methods

Reagents

MLi-2 LRRK2 inhibitor was synthesized by Natalia Shpiro (University of Dundee).

Cell culture

HEK293 cells (ATCC) were cultured in DMEM (Dulbecco s Modified Eagle Medium) (Dulbecco's Modified Eagle Medium, Gibco ™) containing 10% (v/v) foetal calf serum, 2 mM L-glutamine, 100 U/ml penicillin and 100 µg/ml streptomycin at 37°C in a humidified incubator maintaining 5% (v/v) CO_2. Cells were regularly tested for mycoplasma contamination.

Plasmids

All plasmids used in this study were obtained from the MRC PPU Reagents and Services (https://mrcppureagents.dundee.ac.uk). Each LRRK2 variant was confirmed by sequencing at the MRC Sequencing and Services (https://www.dnaseq.co.uk) and the amplified plasmid

preparation quality was validated via agarose gel electrophoresis using ethidium bromide staining. All plasmids are available to request via the MRC PPU Reagents and Services website (https://mrcppureagents.dundee.ac.uk)

DU number	Construct	Plasmid
DU44060	Flag-empty	pCMV5D
DU6841	Flag LRRK2 wildtype	pCMV5
DU10128	Flag LRRK2 D2017A (KD)	pCMV5
DU13826	Flag LRRK2 E10K	pCMV5
DU62019	Flag LRRK2 M100T	pCMV5
DU68340	Flag LRRK2 H115P	pCMV5
DU68326	Flag LRRK2 L119P	pCMV5
DU62020	Flag LRRK2 L153W	pCMV5
DU26913	Flag LRRK2 A211V	pCMV5
DU68327	Flag LRRK2 M262V	pCMV5
DU26914	Flag LRRK2 E334K	pCMV5
DU26911	Flag LRRK2 N363S	pCMV5
DU68328	Flag LRRK2 I388T	pCMV5
DU68329	Flag LRRK2 G393V	pCMV5
DU26842	Flag LRRK2 A419V	pCMV5
DU62596	Flag LRRK2 A459S	pCMV5
DU68330	Flag LRRK2 D478Y	pCMV5
DU68331	Flag LRRK2 I479V	pCMV5
DU13049	Flag LRRK2 K544E	pCMV5
DU26736	Flag LRRK2 N551K	pCMV5
DU62834	Flag LRRK2 K616R	pCMV5
DU26915	Flag LRRK2 M712V	pCMV5
DU62002	Flag LRRK2 S722N	pCMV5
DU68332	Flag LRRK2 I723V	pCMV5
DU26926	Flag LRRK2 P755L	pCMV5

DU26708	Flag LRRK2 R767H	pCMV5
DU68333	Flag LRRK2 T776M	pCMV5
DU62016	Flag LRRK2 R792K	pCMV5
DU26912	Flag LRRK2 R793M	pCMV5
DU26907	Flag LRRK2 I810V	pCMV5
DU26722	Flag LRRK2 S865F	pCMV5
DU26709	Flag LRRK2 S885N	pCMV5
DU62855	Flag LRRK2 Q923H	pCMV5
DU62012	Flag LRRK2 C925Y	pCMV5
DU13164	Flag LRRK2 Q930R	pCMV5
DU68334	Flag LRRK2 D944V	pCMV5
DU13082	Flag LRRK2 S973N	pCMV5
DU62038	Flag LRRK2 R981K	pCMV5
DU62003	Flag LRRK2 S1007T	pCMV5
DU13043	Flag LRRK2 R1067Q	pCMV
DU13044	Flag LRRK2 S1096C	pCMV
DU13988	Flag LRRK2 Q1111H	pCMV
DU13286	Flag LRRK2 I1122V	pCMV5
DU26724	Flag LRRK2 K1138E	pCMV5
DU19010	Flag LRRK2 A1151T	pCMV
DU17133	Flag LRRK2 I1192V	pCMV
DU13045	Flag LRRK2 S1228T	pCMV
DU62001	Flag LRRK2 R1320S	pCMV5
DU62011	Flag LRRK2 R1325Q	pCMV5
DU13046	Flag LRRK2 I1371V	pCMV5
DU26565	Flag LRRK2 R1398H	pCMV5
DU26643	Flag LRRK2 N1437H	pCMV5
DU13078	Flag LRRK2 R1441C	pCMV5

DU13077	Flag LRRK2 R1441G	pCMV
DU13287	Flag LRRK2 R1441H	pCMV
DU62906	Flag LRRK2 R1441S	pCMV5
DU13170	Flag LRRK2 A1442P	pCMV5
DU62501	Flag LRRK2 V1447M	pCMV5
DU62849	Flag LRRK2 A1464G	pCMV5
DU68324	Flag LRRK2 K1468E	pCMV5
DU62848	Flag LRRK2 S1508R	pCMV5
DU62836	Flag LRRK2 S1508G	pCMV5
DU67599	Flag LRRK2 R1514G	pCMV5
DU13047	Flag LRRK2 R1514Q	pCMV5
DU68335	Flag LRRK2 P1542S	pCMV5
DU68336	Flag LRRK2 A1589S	pCMV5
DU19019	Flag LRRK2 V1613A	pCMV5
DU68325	Flag LRRK2 R1628C	pCMV5
DU19007	Flag LRRK2 R1628P	pCMV5
DU26840	Flag LRRK2 M1646T	pCMV5
DU62517	Flag LRRK2 R1677S	pCMV5
DU26486	Flag LRRK2 Y1699C	pCMV5
DU62840	Flag LRRK2 R1725Q	pCMV5
DU17138	Flag LRRK2 R1728H	pCMV5
DU17139	Flag LRRK2 R1728L	pCMV5
DU62839	Flag LRRK2 S1761R	pCMV5
DU17134	Flag LRRK2 L1795F	pCMV5
DU62838	Flag LRRK2 Q1823K	pCMV5
DU13169	Flag LRRK2 M1869T	pCMV5
DU13079	Flag LRRK2 R1941H	pCMV5
DU62837	Flag LRRK2 I1991V	pCMV5

DU13880	Flag LRRK2 Y2006H	pCMV5
DU13080	Flag LRRK2 I2012T	pCMV5
DU10129	Flag LRRK2 G2019S	pCMV5
DU13081	Flag LRRK2 I2020T	pCMV5
DU17135	Flag LRRK2 T2031S	pCMV5
DU26721	Flag LRRK2 N2081D	pCMV5
DU17140	Flag LRRK2 T2141M	pCMV5
DU17141	Flag LRRK2 R2143M	pCMV5
DU62374	Flag LRRK2 D2175H	pCMV5
DU62391	Flag LRRK2 Y2189C	pCMV5
DU62004	Flag LRRK2 N2308D	pCMV5
DU62005	Flag LRRK2 N2313S	pCMV5
DU62502	Flag LRRK2 S2350I	pCMV5
DU62375	Flag LRRK2 T2356I	pCMV5
DU27381	Flag LRRK2 G2385R	pCMV5
DU62376	Flag LRRK2 V2390M	pCMV5
DU26735	Flag LRRK2 M2397T	pCMV5
DU62393	Flag LRRK2 L2439I	pCMV5
DU17142	Flag LRRK2 L2466H	pCMV5
DU30901	Flag LRRK2 T2494I	pCMV5
DU62804	Flag LRRK2 T1647S (S1647S reversed)	pCMV5
DU62832	Flag LRRK2 R1441G T1647S	pCMV5
DU62805	Flag LRRK2 G2019S T1647S	pCMV5
DU68883	Flag LRRK2 Y1699C+G2019S	pCMV5
DU68846	Flag LRRK2 Y1699C+T2031S	pCMV5
DU49303	HA-empty	pCMV5D
DU50222	HA-Rab29	pCMV5D

Cell transfection and lysis

A protocols.io description of our cell transfection (dx.doi.org/10.17504/protocols.io.bw4bpgsn) and cell lysis method (dx.doi.org/10.17504/protocols.io.b5jhq4j6) has previously been described. For LRRK2 variant immunoblot analysis, HEK293 cells were seeded into 6-well plates and transiently transfected at 60-70% confluence using Polyethylenimine (PEI) transfection reagent with Flag-empty, Flag-LRRK2 wildtype or variant plasmids. 2 µg of plasmid and 6 µg of PEI were diluted in 0.5 mL of Opti-MEM™ Reduced serum medium (Gibco™) per single well. Cells were lysed 24 hours post-transfection in an ice-cold lysis buffer containing 50 mM Tris/HCl pH 7.4, 1 mM EGTA, 10 mM 2-glycerophosphate, 50 mM sodium fluoride, 5 mM sodium pyrophosphate, 270 mM sucrose, supplemented with 1 µg/ml microcystin-LR, 1 mM sodium orthovanadate, complete EDTA-free protease inhibitor cocktail (Roche), and 1% (v/v) Triton X-100. Lysates were clarified by centrifugation at 17000 *g* at 4°C for 10 min and supernatants were quantified by Bradford assay.

For LRRK2 variant screen for microtubule association, cells were split into either µ-Plate 24-wells (#1.5 polymer coverslip, black well, flat bottom, ibiTreat; Ibidi) for immunofluorescence or regular 24-well plates for immunoblotting control. Cells were transfected using Polyethylenimine (PEI) transfection with Flag-empty, Flag-LRRK2 wildtype or variant plasmids. 0.6 µg of plasmid and 1.7 µg of PEI in 0.15 mL of Opti-MEM™ per single well. Three hours prior to lysis, cells were treated with 100 nM MLi-2 or 0.1% (v/v) DMSO (vehicle). 48 hours post-transfection, cells for immunofluorescence were fixed for 10 minutes using 4% (v/v) PFA in PBS (Phosphate Buffered Saline), pre-warmed to 37°C and cells for immunoblotting were lysed as above.

Quantitative immunoblot analysis

A protocols.io description of our quantitative immunoblotting protocol has previously been described (dx.doi.org/10.17504/protocols.io.bsgrnbv6). Briefly extracts were mixed with a quarter of a volume of 4x SDS-PAGE loading buffer [250 mM Tris–HCl, pH 6.8, 8% (w/v) SDS, 40% (v/v) glycerol, 0.02% (w/v) bromophenol blue and 5% (v/v) 2-mercaptoethanol] and heated at 95 °C for 5 minutes. Samples were loaded onto NuPAGE 4–12% Bis–Tris Midi Gels (Thermo Fisher Scientific, Cat# WG1402BOX or Cat# WG1403BOX) or self-cast 10% Bis-Tris gels and electrophoresed at 130 V for 2 hours with NuPAGE MOPS SDS running buffer (Thermo Fisher Scientific, Cat# NP0001-02). At the end of electrophoresis, proteins were electrophoretically transferred onto a nitrocellulose membrane (GE Healthcare, Amersham Protran Supported 0.45 µm NC) at 90 V for 90 minutes on ice in transfer buffer (48 mM Tris base and 39 mM glycine supplemented with 20% (v/v) methanol). The membranes were blocked with 5% (w/v) skim milk powder dissolved in TBS-T (50 mM Tris base, 150 mM sodium chloride (NaCl), 0.1% (v/v) Tween 20) at room temperature for 1 hour. Membranes were washed three times with TBS-T and were incubated in primary antibody overnight at 4 °C. Prior to secondary antibody incubation, membranes were washed three times for 15 minutes each with TBS-T. The membranes were incubated with secondary antibody for 1 hour at room temperature. Thereafter, membranes were washed with TBS-T three times with a 15 minute incubation for each wash, and protein bands were acquired *via* near infrared fluorescent detection using the Odyssey CLx imaging system and quantified using Image Studio software.

Antibody target	Company	Catalogue number	Host species	Dilution
LRRK2 (C-terminus)	Antibodies Inc./NeuroMab	75-253	Mouse	1:1000
LRRK2 pSer935	MRC PPU Reagents and Services, University of Dundee	UDD2	Rabbit	1 μg/ml
LRRK2 pSer955	Abcam Inc.	ab169521	Rabbit	1:1000
LRRK2 pSer973	Abcam Inc.	ab181364	Rabbit	1:1000
LRRK2 pSer1292	Abcam Inc.	ab203181	Rabbit	1:2000
LRRK2 pThr1357	Abcam Inc.	ab270606	Rabbit	1:1000
LRRK2 pThr1503	Abcam Inc.	ab154423	Rabbit	1:1000
Rab8A pThr72	Abcam Inc.	ab230260	Rabbit	1:1000
Rab8A	Sigma Aldrich	WH0004218M2	Mouse	1 μg/ml
Rab10 pThr73	Abcam Inc.	ab230261	Rabbit	1:1000
Rab10	Nanotools	0680–100/Rab10-605B11	Mouse	1:500
Rab29 pThr71	Abcam Inc.	ab241062	Rabbit	1:1000
HA	Sigma Aldrich	11867423001	Rat	1:1000
Alpha-tubulin	Cell Signalling Technologies	3873S	Mouse	1:1000

Secondary Antibodies	Company	Catalogue number	Dilution
IRDye 800CW Donkey anti-Rabbit IgG	LI-COR	926-32213	1:10,000
IRDye 800CW Goat anti-Rabbit IgG	LI-COR	926-32211	1:10,000
IRDye 680LT Donkey anti-Mouse IgG	LI-COR	926-68022	1:10,000
IRDye 800CW Donkey anti-Mouse IgG	LI-COR	926-32212	1:10,000
IRDye 680LT Goat anti-Rat IgG	LI-COR	926-68029	1:10,000

Immunoprecipitation kinase assays

A protocols.io description of our LRRK2 immunoprecipitation kinase assay has previously been described (dx.doi.org/10.17504/protocols.io.bw4bpgsn). Briefly, HEK293 cells were transiently transfected with FLAG-LRRK2 wildtype, FLAG-LRRK2 D2017A, and FLAG-tagged LRRK2

variants using polyethylenimine (PEI) and lysed 24 hours post-transfection. Prior to immunoprecipitation, cell lysates were subjected to quantitative immunoblotting to assess the expression of each LRRK2 variant by quantifying total LRRK2 and normalizing to Tubulin. 100 µg cell lysate expressing FLAG-LRRK2 wild type, and the equivalent amount of cell lysate adjusted according to expression of each FLAG-tagged LRRK2 variant, was used to immunoprecipitate LRRK2 with 10 µl anti-FLAG M2 resin for one hour at 4 degrees, and immunoprecipitations were set up in triplicate per dish of cells. Immunoprecipitates were washed three times with lysis buffer supplemented with 300 mM NaCl, and twice with 50 mM Tris/HCl (pH 7.5). Kinase reactions were set up in a total volume of 25 µl, with immunoprecipitated LRRK2 in 50 mM Tris/HCl (pH 7.5), 10 mM $MgCl_2$, 1 mM ATP, in the presence of 5 µg recombinant Rab8A. Kinase reactions were carried out at 30°C for 45 minutes at 1150 rpm. Reactions were terminated by adding 25 µl 4X LDS (lithium dodecyl sulfate) loading buffer to the beads. After heating the reactions at 70°C for 15 minutes, the eluates were collected by centrifugation through a 0.22 µM pore-size Spin-X column and supplemented with 2% (v/v) 2-mercaptoethanol. The kinase reactions were heated at 95°C for 5 minutes, then subjected to quantitative immunoblot analysis. Membranes were developed using the Licor Odyssey CLx scan Western Blot imaging system and quantified using Image Studio.

Immunofluorescence, imaging, and cell counting and quantitation of Microtubule binding

A protocols.io description of the Immunofluorescence-based method that we used to assess LRRK2 association with microtubules in HEK293 cells has been described (dx.doi.org/10.17504/protocols.io.b5jhq4j6). Cells were fixed in 4% (w/v) paraformaldehyde (Sigma Aldrich #P6148) in PBS, pH 7.4 for 10 minutes, followed by permeabilisation using 1% (v/v) NP-40 in PBS for 10 minutes. Cells were then blocked in 1% (w/v) bovine serum albumin in PBS for 1 hour at room temperature. Blocked cells were incubated with Flag M2 (1:1000) and β-tubulin (1:500) antibodies for 2 hours at 37ºC. Cells were washed 3 times (15 minutes each) with 0.2% (w/v) bovine serum albumin in PBS and incubated with secondary antibodies (goat-anti-mouse Alexa Fluor 488 and goat-anti-rabbit Alexa Fluor 594, Thermo Fisher Scientific, 1:500) and 1 µg/ml DAPI for 1 hour at room temperature in the dark. Cells were washed 3 times (15 minutes each) with 0.2% (w/v) bovine serum albumin in PBS and were kept in PBS at 4° C until imaging. Plates were imaged on the Zeiss LSM 710 or 880 laser scanning microscopes using the x40 EC Plan-Neofluar (NA 1.3) objective with a zoom of 0.6 and optical section thickness of 1.0 µm (image size 2048x2048 pixels, pixel size 0.173 mm). 4-6 randomly selected fields with Alexa Fluor 488-positive cells were collected for each well blinded to LRRK2 variant and treatment conditions. For further cell counting, LRRK2 variant and treatment condition were blinded from the counter by renaming the image files using a simple Python code script. Cells containing any filamentous shapes of the Alexa Fluor 488 signal were counted as “filamentous,” ones without filamentous signal but with punctate staining were counted as “punctate,” and the remaining cells with fully cytosolic signal were counted as “cytosolic.” DAPI and β-tubulin signal was used to make sure only cells containing a single nucleus were counted, avoiding cells that have not finished dividing or are multi-nuclear. Variants with a statistically significant and largest effect on inhibitor-induced LRRK2 filament formation (<10% of LRRK2 signal-positive cells after MLi-2 treatment compared to the 34.7% of MLi-2 treated wildtype LRRK2 cells) were labelled as the “Strongest impact” group, the remaining variants with a statistically significant decrease

in LRRK2 filament formation (<21%) were labelled as "Moderate impact" and the remaining variants were labelled as "Microtubule binding not significantly impacted".

Immunoblotting data analysis

Immunoblotting data (acquired using a LI-COR CLx Western Blot imaging system) were quantified using Image Studio. Quantified data were plotted with GraphPad Prism. For the primary screen, data from up to 6 independent biological replicates were combined (all normalized to the wildtype LRRK2 values for each replicate). For the secondary screen, data from 2 independent biological replicates (each performed in duplicate) were combined (all normalized to the wildtype LRRK2 values for each replicate). For the immunoblotting data obtained from the primary screen, outliers of LRRK2 variant activity were determined using an arbitrary cut-off of LRRK2 expression 1.9-fold higher or lower than wildtype LRRK2 expression (designated as 1) and are presented in Figure 1C and Figure 2 as open circle data points and excluded from the variant mean. LRRK2 variants that were expressed less than ~2 relative to wildtype LRRK2, or greater than ~0.5 relative to wildtype LRRK2, were considered true representations of variant activity and are presented in Figure 1C and Figure 2 as closed circles.

Statistical analysis

Gathered data either from immunoblotting or cell counting was analysed using GraphPad Prism 8. One- or multi-way ANOVA with Dunnett's multiple comparisons post-hoc test was used to determine statistical significance and approximate p values for each value compared to the control mean – wildtype LRRK2.

Data Availability

All the primary data that is presented in this study has been deposited on the Zenodo data repository (10.5281/zenodo.6401194) and can be requested in electronic form by contacting Dario Alessi (d.r.alessi@dundee.ac.uk). All plasmids and antibodies (and associated datasheets) generated at the MRC Protein Phosphorylation and Ubiquitylation Unit at the University of Dundee can be requested through our reagent's website https://mrcppureagents.dundee.ac.uk/.

Competing Interests

The authors declare no competing interests.

Funding

A.F.K. was generously supported by a Parkinson's UK Studentship (H-1701). D.R.A lab is funded by UK Medical Research Council [grant number MC_UU_00018/1], the pharmaceutical companies supporting the Division of Signal Transduction Therapy Unit (Boehringer Ingelheim, GlaxoSmithKline, Merck KGaA.), and the joint efforts of The Michael J. Fox Foundation for Parkinson's Research (MJFF) and Aligning Science Across Parkinson's (ASAP) initiative. MJFF administers the grant (ASAP-000463) on behalf of ASAP and itself. E.S. was supported by a CSO Scottish Senior Clinical Academic Fellowship.

Acknowledgements

We thank Axel Knebel for purifying recombinant Rab8A, Natalia Shpiro for generating MLi-2, and Suzanne Pfeffer for helpful discussions. We also thank the excellent technical support of

the MRC protein phosphorylation and ubiquitylation unit (PPU) DNA sequencing service (coordinated by Gary Hunter), the MRC-PPU tissue culture team (coordinated by Edwin Allen), MRC-PPU Reagents and Services antibody and protein purification teams (coordinated by Dr James Hastie). This research was funded in part by Aligning Science Across Parkinson's [ASAP-000463] through the Michael J. Fox Foundation for Parkinson's Research (MJFF). For the purpose of open access, the authors have applied a CC BY public copyright license to all Author Accepted Manuscripts arising from this submission.

Author contributions

A.F.K., E.P., F.T. planned and performed all experimental work, analysed data, prepared figures, and helped write manuscript. S.V.M performed the structural analysis related to Fig 8 and SFig 7. M.L. performed most of the cloning required to generate LRRK2 variants. A.R.P. undertook microscopy studies for the microtubule binding analysis. S.P. and E.S. provided advice and helped with the selection of LRRK2 variants. D.R.A contributed to conceptualization of project, data analysis, writing manuscript and supervised the work.

References

1 Paisán-Ruíz, C., Jain, S., Evans, E. W., Gilks, W. P., Simón, J., van der Brug, M., De Munain, A. L., Aparicio, S., Gil, A. M., Khan, N., et al. (2004) Cloning of the gene containing mutations that cause PARK8-linked Parkinson's disease. Neuron 44, 595–600.

2 Zimprich, A., Biskup, S., Leitner, P., Lichtner, P., Farrer, M., Lincoln, S., Kachergus, J., Hulihan, M., Uitti, R. J., Calne, D. B., et al. (2004) Mutations in LRRK2 cause autosomal-dominant parkinsonism with pleomorphic pathology. Neuron 44, 601–607.

3 Alessi, D. R. and Sammler, E. (2018) LRRK2 kinase in Parkinson's disease. 360, 36–37.

4 Hui, K. Y., Fernandez-Hernandez, H., Hu, J., Schaffner, A., Pankratz, N., Hsu, N. Y., Chuang, L. S., Carmi, S., Villaverde, N., Li, X., et al. (2018) Functional variants in the LRRK2 gene confer shared effects on risk for Crohn's disease and Parkinson's disease. Sci. Transl. Med. 10.

5 Usmani, A., Shavarebi, F. and Hiniker, A. (2021) The Cell Biology of LRRK2 in Parkinson's Disease. Mol. Cell. Biol. 41.

6 Leschziner, A. E. and Reck-Peterson, S. L. (2021) Structural Biology of LRRK2 and its Interaction with Microtubules. Mov. Disord. 36, 2494–2504.

7 Taylor, M. and Alessi, D. R. (2020) Advances in elucidating the function of leucine-rich repeat protein kinase-2 in normal cells and Parkinson's disease. Curr. Opin. Cell Biol., Elsevier Ltd 63, 102–113.

8 Myasnikov, A., Zhu, H., Hixson, P., Xie, B., Yu, K., Pitre, A., Peng, J. and Sun, J. (2021) Structural analysis of the full-length human LRRK2. Cell, Elsevier Inc. 184, 3519-3527.e10.

9 Deniston, C. K., Salogiannis, J., Mathea, S., Snead, D. M., Lahiri, I., Matyszewski, M., Donosa, O., Watanabe, R., Böhning, J., Shiau, A. K., et al. (2020) Structure of LRRK2 in Parkinson's disease and model for microtubule interaction. Nature.

10 Snead, D. M., Matyszewski, M., Dickey, A. M., Lin, Y. X. and Andres, E. (2022) Structural basis for Parkinson's Disease-linked LRRK2's binding to microtubules. bioRxiv 1–27.

11 Liu, Z., Bryant, N., Kumaran, R., Beilina, A., Abeliovich, A., Cookson, M. R. and West, A. B. (2018) LRRK2 phosphorylates membrane-bound Rabs and is activated by GTP-bound Rab7L1 to promote recruitment to the trans-Golgi network. Hum Mol Genet 27, 385–395.

12 Purlyte, E., Dhekne, H. S., Sarhan, A. R., Gomez, R., Lis, P., Wightman, M., Martinez, T. N., Tonelli, F., Pfeffer, S. R. and Alessi, D. R. (2018) Rab29 activation of the Parkinson's disease-associated LRRK2 kinase. EMBO J 37, 1–18.

13 McGrath, E., Waschbüsch, D., Baker, B. M. and Khan, A. R. (2019) LRRK2 binds to the Rab32 subfamily in a GTP-dependent manner via its armadillo domain. Small GTPases, Taylor & Francis 1–14.

14 Steger, M., Tonelli, F., Ito, G., Davies, P., Trost, M., Vetter, M., Wachter, S., Lorentzen, E., Duddy, G., Wilson, S., et al. (2016) Phosphoproteomics reveals that Parkinson's disease kinase LRRK2 regulates a subset of Rab GTPases. Elife 5, e12813.

15 Steger, M., Diez, F., Dhekne, H. S., Lis, P., Nirujogi, R. S., Karayel, O., Tonelli, F., Martinez, T. N., Lorentzen, E., Pfeffer, S. R., et al. (2017) Systematic proteomic analysis of LRRK2-mediated Rab GTPase phosphorylation establishes a connection to ciliogenesis. Elife 6, e31012.

16 Pfeffer, S. R. (2018, November 22) LRRK2 and Rab GTPases. Biochem. Soc. Trans., Portland Press Ltd.

17 Dhekne, H. S., Yanatori, I., Gomez, R. C., Tonelli, F., Diez, F., Schüle, B., Steger, M., Alessi, D. R. and Pfeffer, S. R. (2018) A pathway for parkinson's disease LRRK2 kinase to block primary cilia and sonic hedgehog signaling in the brain. Elife, eLife Sciences Publications Ltd 7.

18 Bonet-Ponce, L., Beilina, A., Williamson, C. D., Lindberg, E., Kluss, J. H., Saez-Atienzar, S., Landeck, N., Kumaran, R., Mamais, A., Bleck, C. K. E., et al. (2020) LRRK2 mediates tubulation and vesicle sorting from lysosomes. Sci. Adv. 6, 1–15.

19 Waschbüsch, D., Purlyte, E., Pal, P., McGrath, E., Alessi, D. R. and Khan, A. R. (2020) Structural Basis for Rab8a Recruitment of RILPL2 via LRRK2 Phosphorylation of Switch 2. Structure, Cell Press 28, 406–417.

20 Dhekne, H. S., Yanatori, I., Vides, E. G., Sobu, Y., Diez, F., Tonelli, F. and Pfeffer, S. R. (2021) LRRK2-phosphorylated Rab10 sequesters Myosin Va with RILPL2 during ciliogenesis blockade. Life Sci. Alliance 4, 1–16.

21 Berndsen, K., Lis, P., Yeshaw, W. M., Wawro, P. S., Nirujogi, R. S., Wightman, M., Macartney, T., Dorward, M., Knebel, A., Tonelli, F., et al. (2019) PPM1H phosphatase counteracts LRRK2 signaling by selectively dephosphorylating rab proteins. Elife, eLife Sciences Publications Ltd 8.

22 Watanabe, R., Buschauer, R., Böhning, J., Audagnotto, M., Lasker, K., Wen Lu, T., Boassa, D., Taylor, S. S. and Villa, E. (2020) The In situ Structure of Parkinson's Disease-Linked LRRK2. Biophys. J. 118, 486a.

23 Schmidt, S. H., Knape, M. J., Boassa, D., Mumdey, N., Kornev, A. P., Ellisman, M. H., Taylor, S. S. and Herberg, F. W. (2019) The dynamic switch mechanism that leads to activation of LRRK2 is embedded in the DFGψ motif in the kinase domain. Proc. Natl. Acad. Sci. U. S. A., National Academy of Sciences 116, 14979–14988.

24 Kett, L. R., Boassa, D., Ho, C. C. Y., Rideout, H. J., Hu, J., Terada, M., Ellisman, M. and Dauer, W. T. (2012) LRRK2 Parkinson disease mutations enhance its microtubule association. Hum. Mol. Genet. 21, 890–899.

25 Dzamko, N., Deak, M., Hentati, F., Reith, A. D., Prescott, A. R., Alessi, D. R. and Nichols, R. J. (2010) Inhibition of LRRK2 kinase activity leads to dephosphorylation of Ser 910/Ser935, disruption of 14-3-3 binding and altered cytoplasmic localization. Biochem. J. 430, 405–413.

26 Doggett, E. A., Zhao, J., Mork, C. N., Hu, D. and Nichols, R. J. (2012) Phosphorylation of LRRK2 serines 955 and 973 is disrupted by Parkinson's disease mutations and LRRK2 pharmacological inhibition. J. Neurochem. 120, 37–45.

27 Tasegian, A., Singh, F., Ganley, I. G., Reith, A. D. and Alessi, D. R. (2021) Impact of Type II LRRK2 inhibitors on signaling and mitophagy. Biochem. J. 478, 3555–3573.

28 Sheng, Z., Zhang, S., Bustos, D., Kleinheinz, T., Le Pichon, C. E., Dominguez, S. L., Solanoy, H. O., Drummond, J., Zhang, X., Ding, X., et al. (2012) Ser1292 autophosphorylation is an indicator of LRRK2 kinase activity and contributes to the cellular effects of PD mutations. Sci. Transl. Med. 4, 164ra161.

29 Bardien, S., Lesage, S., Brice, A. and Carr, J. (2011) Genetic characteristics of leucine-rich repeat kinase 2 (LRRK2) associated Parkinson's disease. Park. Relat. Disord., Elsevier Ltd 17, 501–508.

30 Gilks, W., Abousleiman, P., Gandhi, S., Jain, S., Singleton, A., Lees, A., Shaw, K., Bhatia, K., Bonifati, V. and Quinn, N. (2005) A common mutation in idiopathic Parkinson's disease. Lancet 365, 415–416.

31 Di Fonzo, A., Rohé, C. F., Ferreira, J., Chien, H. F., Vacca, L., Stocchi, F., Guedes, L., Fabrizio, E., Manfredi, M., Vanacore, N., et al. (2005) A frequent LRRK2 gene mutation associated with autosomal dominant Parkinson's disease. Lancet 365, 412–415.

32 Di Fonzo, A., Wu-Chou, Y. H., Lu, C. S., Van Doeselaar, M., Simons, E. J., Rohé, C. F., Chang, H. C., Chen, R. S., Weng, Y. H., Vanacore, N., et al. (2006) A common missense variant in the LRRK2 gene, Gly2385Arg, associated with Parkinson's disease risk in Taiwan. Neurogenetics 7, 133–138.

33 Zhang, P., Fan, Y., Ru, H., Wang, L., Magupalli, V. G., Taylor, S. S., Alessi, D. R. and Wu, H. (2019) Crystal structure of the WD40 domain dimer of LRRK2. Proc. Natl. Acad. Sci. U. S. A. 116, 1579–1584.

34 Farrer, M. J., Stone, J. T., Lin, C. H., Dächsel, J. C., Hulihan, M. M., Haugarvoll, K., Ross, O. A. and Wu, R. M. (2007) LRRK2 G2385R is an ancestral risk factor for Parkinson's disease in Asia. Park. Relat. Disord. 13, 89–92.

35 Wang, X., Negrou, E., Maloney, M. T., Bondar, V. V., Andrews, S. V., Montalban, M., Llapashtica, C., Maciuca, R., Nguyen, H., Solanoy, H., et al. (2021) Understanding LRRK2

kinase activity in preclinical models and human subjects through quantitative analysis of LRRK2 and pT73 Rab10. Sci. Rep., Nature Publishing Group UK 11, 1–17.

36 Ross, O. A., Soto-Ortolaza, A. I., Heckman, M. G., Aasly, J. O., Abahuni, N., Annesi, G., Bacon, J. A., Bardien, S., Bozi, M., Brice, A., et al. (2011) Association of LRRK2 exonic variants with susceptibility to Parkinson's disease: A case-control study. Lancet Neurol. 10, 898–908.

37 Trabzuni, D., Ryten, M., Emmett, W., Ramasamy, A., Lackner, K. J., Zeller, T., Walker, R., Smith, C., Lewis, P. A., Mamais, A., et al. (2013) Fine-Mapping, Gene Expression and Splicing Analysis of the Disease Associated LRRK2 Locus. PLoS One 8.

38 Bryant, N., Malpeli, N., Ziaee, J., Blauwendraat, C., Liu, Z. and West, A. B. (2021) Identification of LRRK2 missense variants in the accelerating medicines partnership Parkinson's disease cohort. Hum. Mol. Genet. 30, 454–466.

39 Ioannidis, N. M., Rothstein, J. H., Pejaver, V., Middha, S., McDonnell, S. K., Baheti, S., Musolf, A., Li, Q., Holzinger, E., Karyadi, D., et al. (2016) REVEL: An Ensemble Method for Predicting the Pathogenicity of Rare Missense Variants. Am. J. Hum. Genet., American Society of Human Genetics 99, 877–885.

40 Liu, X., Jian, X. and Boerwinkle, E. (2013) dbNSFP v2.0: A database of human non-synonymous SNVs and their functional predictions and annotations. Hum. Mutat. 34, 2393–2402.

41 Lis, P., Burel, S., Steger, M., Mann, M., Brown, F., Diez, F., Tonelli, F., Holton, J. L., Ho, P. W., Ho, S. L., et al. (2018) Development of phospho-specific Rab protein antibodies to monitor in vivo activity of the LRRK2 Parkinson's disease kinase. Biochem. J. 475, 1–22.

42 Richards, S., Aziz, N., Bale, S., Bick, D., Das, S., Gastier-Foster, J., Grody, W. W., Hegde, M., Lyon, E., Spector, E., et al. (2015) Standards and guidelines for the interpretation of sequence variants: A joint consensus recommendation of the American College of Medical Genetics and Genomics and the Association for Molecular Pathology. Genet. Med., Elsevier Masson SAS 17, 405–424.

43 Ashkenazy, H., Abadi, S., Martz, E., Chay, O., Mayrose, I., Pupko, T. and Ben-Tal, N. (2016) ConSurf 2016: an improved methodology to estimate and visualize evolutionary conservation in macromolecules. Nucleic Acids Res. 44, W344–W350.

44 Ross, O. A., Wu, Y. R., Lee, M. C., Funayama, M., Chen, M. L., Soto, A. I., Mata, I. F., Lee-Chen, G. J., Chiung, M. C., Tang, M., et al. (2008) Analysis of Lrrk2 R1628P as a risk factor for Parkinson's disease. Ann. Neurol. 64, 88–92.

45 Nixon-Abell, J., Berwick, D. C., Grannó, S., Spain, V. A., Blackstone, C. and Harvey, K. (2016) Protective LRRK2 R1398H variant enhances GTPase and Wnt signaling activity. Front. Mol. Neurosci. 9, 1–13.

46 Jaleel, M., Nichols, R. J., Deak, M., Campbell, D. G., Gillardon, F., Knebel, A. and Alessi, D. R. (2007) LRRK2 phosphorylates moesin at threonine-558: Characterization of how Parkinson's disease mutants affect kinase activity. Biochem. J. 405, 307–317.

47 Nichols, R. J., Dzamko, N., Morrice, N. A., Campbell, D. G., Deak, M., Ordureau, A., Macartney, T., Tong, Y., Shen, J., Prescott, A. R., et al. (2010) 14-3-3 Binding to LRRK2 is disrupted by multiple Parkinson's disease-associated mutations and regulates cytoplasmic localization. Biochem. J. 430, 393–404.

48 Kamikawaji, S., Ito, G., Sano, T. and Iwatsubo, T. (2013) Differential effects of familial parkinson mutations in LRRK2 revealed by a systematic analysis of autophosphorylation. Biochemistry 52, 6052–6062.

49 Ito, G., Fujimoto, T., Kamikawaji, S., Kuwahara, T. and Iwatsubo, T. (2014) Lack of correlation between the kinase activity of LRRK2 harboring kinase-modifying mutations and its phosphorylation at Ser910, 935, and Ser955. PLoS One 9.

50 Fujimoto, T., Kuwahara, T., Eguchi, T., Sakurai, M., Komori, T. and Iwatsubo, T. (2018) Parkinson's disease-associated mutant LRRK2 phosphorylates Rab7L1 and modifies trans-Golgi morphology. Biochem Biophys Res Commun 495, 1708–1715.

51 Jumper, J., Evans, R., Pritzel, A., Green, T., Figurnov, M., Ronneberger, O., Tunyasuvunakool, K., Bates, R., Žídek, A., Potapenko, A., et al. (2021) Highly accurate protein structure prediction with AlphaFold. Nature, Springer US 596, 583–589.

52 Taylor, S. S., Kaila-Sharma, P., Weng, J. H., Aoto, P., Schmidt, S. H., Knapp, S., Mathea, S. and Herberg, F. W. (2020) Kinase Domain Is a Dynamic Hub for Driving LRRK2 Allostery. Front. Mol. Neurosci. 13, 1–12.

53 Weng, J.-H., Aoto, P. C., Lorenz, R., Wu, J., Schmidt, S. H., Manschwetus, J. T., Kaila-Sharma, P., Silletti, S., Mathea, S., Chatterjee, D., et al. (2022) LRRK2 dynamics analysis identifies allosteric control of the crosstalk between its catalytic domains. PLOS Biol. 20.

54 Schmidt, S. H., Weng, J. H., Aoto, P. C., Boassa, D., Mathea, S., Silletti, S., Hu, J., Wallbott, M., Komives, E. A., Knapp, S., et al. (2021) Conformation and dynamics of the kinase domain drive subcellular location and activation of LRRK2. Proc. Natl. Acad. Sci. U. S. A. 118.

55 Tolosa, E., Vila, M., Klein, C. and Rascol, O. (2020) LRRK2 in Parkinson disease: challenges of clinical trials. Nat. Rev. Neurol., Springer US 16, 97–107.

56 Pillay, N. S., Ross, O. A., Christoffels, A. and Bardien, S. (2022) Current Status of Next-Generation Sequencing Approaches for Candidate Gene Discovery in Familial Parkinson´s Disease. Front. Genet. 13.

57 Riboldi, G. M. and Di Fonzo, A. B. (2019) GBA, Gaucher Disease, and Parkinson's Disease: From Genetic to Clinic to New Therapeutic Approaches. Cells 8, 1–16.

Figure Legends

Figure 1. Domain location of 98 LRRK2 variants and experimental workflow to assess LRRK2 variant activity by quantitative immunoblotting.
(A) LRRK2 domain structure highlighting 98 PD and CD associated variants within the Armadillo (ARM), Ankyrin (ANK), Leucine Rich Repeats (LRR), Ras of complex proteins (ROC), C-terminal of Roc A and B (COR_A, COR_B), Kinase (KIN), and WD40 domains. The LRRK2 variants located in the linker region between the hinge-helix (HH) and LRR domain are listed in black. (B) Workflow schematic outlining the characterisation of 98 LRRK2 variants in a HEK293 overexpression system, followed by quantitative immunoblotting and quantitation of LRRK2 activity relative to wildtype LRRK2. (C) FLAG-tagged LRRK2 wildtype, kinase dead (KD = D2017A), and the indicated variants were transiently expressed in HEK293 cells. 24 hours post-transfection, cells were lysed and analysed by quantitative immunoblotting (as in

Supplementary Figure 1). Quantified immunoblotting data are presented as ratios of pRab10^{Thr73}/total Rab10, normalized to the average of LRRK2 wildtype values for each replicate (mean ± SD). Combined immunoblotting data from up to 6 independent biological replicates are shown. Dashed lines segment the graphs into corresponding regions of LRRK2 as listed in the domain schematic.

Figure 2. Quantitative analysis of phosphorylation and expression of 98 PD and CD-associated LRRK2 variants assessed in primary screens. FLAG-tagged LRRK2 wildtype, kinase dead (KD = D2017A), and the indicated variants were transiently expressed in HEK293 cells. 24 hours post-transfection, cells were lysed and analysed by quantitative immunoblotting (as in Supplementary Figure 1). Quantified immunoblotting data are presented as ratios of phospho-LRRK2 Ser1292/total LRRK2 (A), phospho-LRRK2 Ser935 (B), and total LRRK2/Tubulin (C), normalized to the average of LRRK2 wildtype values for each replicate (mean ± SD). Combined immunoblotting data from 6 independent biological replicates are shown. Dashed lines segment the graphs into corresponding regions of LRRK2 as listed in the domain schematic.

Figure 3. 22 LRRK2 variants with mutations spanning multiple domains significantly augment LRRK2-mediated Rab10^{Thr73} phosphorylation. A) FLAG-tagged LRRK2 wildtype, kinase dead (KD = D2017A) and the indicated variants were transiently expressed in HEK293 cells. 24 hours post-transfection, cells were lysed and analysed by quantitative immunoblotting using the indicated antibodies. Data quantification is shown in panels C-E. (B) Domain schematic of LRRK2 highlighting the position of the 22 LRRK2 variants selected for further analysis. (C-E) Quantified immunoblotting data are presented as ratios of pRab10^{Thr73}/total Rab10 (C), phospho-LRRK2 Ser1292/total LRRK2 (D), phospho-LRRK2 Ser935/total LRRK2, phospho-LRRK2 Ser955/total LRRK2, or phospho-LRRK2 Ser973/total LRRK2 (E), normalized to the average of LRRK2 wildtype values for each replicate (mean ± SD). Combined immunoblotting data from 2 independent biological replicates (each performed in duplicate) are shown. Data were analysed using one-way ANOVA with Dunnett's multiple comparisons test, and statistical significance was represented with p-values (*$p < 0.05$, ** $p < 0.01$, *** $p < 0.001$, **** $p < 0.0001$).

Figure 4. COR$_B$ and kinase domain LRRK2 variants enhance *in vitro* LRRK2 kinase activity against recombinant Rab8A. (A) Workflow schematic outlining the immunoprecipitation kinase assay method employed to assess *in vitro* kinase activity of LRRK2 variants against recombinant Rab8A. Kinase reaction products were analysed by quantitative immunoblotting (as in Supplementary Figure 3, Supplementary Figure 4 and Supplementary Figure 5). (B-D) Data obtained from quantitative immunoblotting analysis of FLAG-LRRK2 immunoprecipitation kinase reactions for the indicates variants are presented as ratios of phospho-Rab8A Thr72/total Rab8A (B), phospho-LRRK2 Ser1292/total LRRK2 (C), and phospho-LRRK2 Thr1357/total LRRK2 (D) normalised to the average of LRRK2 wildtype values (mean ± SD). (E) Data obtained from quantitative immunoblotting analysis of FLAG-LRRK2 immunoprecipitation kinase reactions for the indicates variants are presented as ratios of phospho-Rab8A/total Rab8A, phospho-LRRK2 Ser1292/total LRRK2, relative to the average of LRRK2 wildtype values (mean ± SD).

Figure 5. Selected LRRK2 variants are activated by Rab29. FLAG-tagged LRRK2 wildtype, kinase dead (KD = D2017A) and the indicated variants were transiently expressed in HEK293 cells with HA empty vector or HA-Rab29. 24 hours post-transfection, cells were lysed and analysed by quantitative immunoblotting (as in Supplementary Figure 6). (A-C) Quantified immunoblotting data are presented as ratios of phospho-Rab10/total Rab10 (A), phospho-LRRK2 Ser1292/total LRRK2 (B), phospho-LRRK2 Ser935/total LRRK2 (C), normalized to the average of LRRK2 wildtype values for each replicate (mean ± SD). Combined immunoblotting data from 2 independent biological replicates (each performed in duplicate) are shown.

Figure 6. Impact of 98 LRRK2 variants on Type I inhibitor-induced microtubule association. HEK293 cells transiently transfected with FLAG-tagged LRRK2 wildtype, kinase dead (KD = D2017A) or the indicated variants were treated with 100 nM MLI-2 (or DMSO, control vehicle) for 3 hours to induce microtubule association. Cells were then fixed and subjected to immunofluorescent microscopy imaging of Flag-tagged LRRK2. Data are presented as % of LRRK2 signal-positive cells that show filamentous LRRK2. Two-way ANOVA with the Dunnett's multiple comparisons test was used to evaluate the statistical significance of the results (p values marked on the graph comparing the variant MLI-2-treated group to the WT MLI-2 treated group: * $p<0.05$, ** $p<0.01$, *** $p<0.001$, **** $p<0.0001$. None of the DMSO treated groups showed statistically significant differences from the WT group). Data are arranged by % of cells with filamentous LRRK2 signal upon MLI-2 treatment (low to high).

Figure 7. Correlation between activating LRRK2 mutations and high REVEL pathogenicity prediction or high evolutionary amino acid conservation scores. (A) Schematic summarizing biochemical data of 98 LRRK2 variants and categorisation of variants based on Rab10 phosphorylation, LRRK2 Ser1292 phosphorylation, and biomarker phosphorylation. Variants that enhance *in vitro* LRRK2 kinase activity or block MLi-2 induced microtubule binding are marked with a superscript highlighted in red. (B) LRRK2 orthologue sequences were acquired from OrthoDB. Orthologue sequences were aligned using MAFFT. The multiple sequence alignment of LRRK2 orthologues was submitted to the ConSurf server to determine evolutionary conservation scores for LRRK2 amino acids (1 is low conservation and 9 is high conservation). Conservation scores were plotted against $pRab10^{Thr73}$/total Rab10 ratios acquired for each LRRK2 variant that were normalized to wildtype. Activating variants ($pRab10^{Thr73}$> 1.5-fold relative to wildtype) are marked in green, low activity variants (similar to kinase inactive LRRK2) are marked in red, protective variants are marked in yellow, and variants that block MLi-2 induced microtubule binding are represented with an open circle. (C) REVEL scores for LRRK2 variants were acquired from Bryant et al 2021 or through the online pathogenicity prediction tool http://database.liulab.science/dbNSFP. REVEL scores were plotted against phospho-Rab10/total Rab10 ratios acquired for each LRRK2 variant that were normalized to wildtype. High activity variants (phospho-Rab10 > 1.5-fold relative to wildtype) are marked in green, low activity variants (similar to kinase inactive LRRK2) are marked in red, protective variants are marked in yellow, and variants that block MLI-2 induced microtubule binding are represented with an open circle. The REVEL pathogenicity threshold is marked with a dashed line (0.6). Above this line are variants predicted to be "likely pathogenic or damaging," and variants below this line are predicted to be "likely benign."

Figure 8. Structural analysis of identified activating LRRK2 variants. (A) Schematic domain overview of LRRK2 with domain boundaries. (B) Cartoon representation of LRRK2 [558-2527] with domains coloured as in A. Domain interfaces harbouring activating mutations and kinase domain are indicated by black arrows. (C) Schematic representation of LRRK2 domains as viewed in B. (D-K) Detailed views of LRRK2 variants in kinase active site (D), domain interfaces (E-K), colouring as in A and variants highlighted in magenta. Second LRRK2 molecule of dimer shown in grey (F, K). (J) R1728 side chain modelled in PyMOL shown as semi-transparent stick model. Distance measurements in Å are indicated by dark grey dashed lines. (L) Alphafold model of LRRK2 ARM domain coloured by local confidence score (pLDDT) with variant residues shown as stick models. LRRK2 structures used are PDB 7LI4 (B, D, E, G-J), PDB 7LIH (F), PDB 6DLO (K), AFDB AF-Q5S007-F1_v1 (L)

Supplementary Figure 1. Primary quantitative immunoblot screen to assess activity of 98 PD and CD-associated LRRK2 variants. FLAG-tagged LRRK2 wildtype, kinase dead (KD = D2017A) and the indicated 98 LRRK2 variants were transiently expressed in HEK293 cells. Cells were lysed 24 hours post-transfection and analysed by quantitative immunoblotting using the indicated antibodies. Immunoblot figure is representative of 6 independent biological replicates. Quantification of the combined immunoblotting data from all replicates is presented in Fig 1C, Figure 2A, Figure 2B and Figure 2C.

Supplementary Figure 2. Quantitative analysis of biomarker phosphorylation of 98 PD and CD-associated LRRK2 variants assessed in primary immunoblot screens. FLAG-tagged LRRK2 wildtype, kinase dead (KD = D2017A) and the indicated 98 LRRK2 variants were transiently expressed in HEK293 cells. Cells were lysed 24 hours post-transfection and analysed by quantitative immunoblotting. Quantified immunoblotting data are presented as the ratio of LRRK2 pSer955/total LRRK2 (A) and LRRK2 pSer973/total LRRK2 (B), normalized to the average of LRRK2 wildtype values for each replicate (mean ± SD). Dashed lines segment the graphs into the corresponding regions of LRRK2 as listed in the domain schematic above panel.

Supplementary Figure 3. Analysis of *in vitro* LRRK2 kinase activity against recombinant Rab8A of selected LRRK2 variants. FLAG-tagged LRRK2 wildtype, kinase dead (KD = D2017A) and the indicated LRRK2 variants were transiently expressed in HEK293 cells for 24 hours. (A) Whole cell lysates were analysed by quantitative immunoblotting using the indicated antibodies. (B) FLAG-LRRK2 was immunoprecipitated from whole cell lysates and subjected to an *in vitro* kinase reaction in the presence of recombinant Rab8A. Kinase reaction products were analysed by quantitative immunoblotting using the indicated antibodies.

Supplementary Figure 4. COR_B and kinase domain LRRK2 variants reproducibly enhance *in vitro* LRRK2 kinase activity. FLAG-tagged LRRK2 wildtype, kinase dead (KD = D2017A) and the indicated LRRK2 variants were transiently expressed in HEK293 cells for 24 hours. (A) Whole cell lysates were analysed by quantitative immunoblotting using the indicated antibodies. (B) FLAG-LRRK2 was immunoprecipitated from whole cell lysates and subjected to an *in vitro* kinase reaction in the presence of recombinant Rab8A. Kinase reaction products were analysed by quantitative immunoblotting using the indicated antibodies. Quantified immunoblotting data are presented as ratios of phospho-LRRK2 Thr1357/total

LRRK2, phospho-LRRK2 Thr1503/total LRRK2, or phospho-Rab8A Thr72/total Rab8A, normalized to the average of wildtype LRRK2 values (mean ± SD).

Supplementary Figure 5. Combination of COR_B and kinase domain LRRK2 mutations further enhances *in vitro* LRRK2 kinase activity. FLAG-tagged LRRK2 wildtype, kinase dead (KD = D2017A) and the indicated LRRK2 variants were transiently expressed in HEK293 cells for 24 hours. (A) Whole cell lysates were analysed by quantitative immunoblotting using the indicated antibodies. Quantified immunoblotting data are presented as ratios of phospho-LRRK2 Ser935/total LRRK2, phospho-Rab10 Thr73/total Rab10, and total LRRK2/Tubulin. (B) FLAG-LRRK2 was immunoprecipitated from whole cell lysates and subjected to an *in vitro* kinase reaction in the presence of recombinant Rab8A. Kinase reaction products were analysed by quantitative immunoblotting using the indicated antibodies. Quantified data are presented in Fig 4E.

Supplementary Figure 6. Activation of selected LRRK2 variants by Rab29. FLAG-tagged LRRK2 wildtype, kinase dead (KD = D2017A) and the indicated variants were transiently expressed in HEK293 cells with HA empty vector or HA-Rab29. 24 hours post-transfection, cells were lysed and analysed by quantitative immunoblotting with the indicated antibodies. Quantified data are presented in Figure 5.

Supplementary Figure 7. Superposition of full-length LRRK2 electron density map (PDB 7LHW) on Alphafold LRRK2 model. Alphafold model of LRRK2 ARM domain has a high local confidence score (pLDDT) and agrees well with experimental data. The ARM domain of the Alphafold model of LRRK2 (residues 159-511, AFDB AF-Q5S007-F1-model_v1) was coloured by pLDDT and fitted into the experimental cryo-EM map of full-length LRRK2 (grey, EMD-23352) using the UCSF ChimeraX “Fit in Map” tool. The remaining C-terminal LRRK2 residues [540-2527] are shown in green (PDB 7LHW).

Figure 1

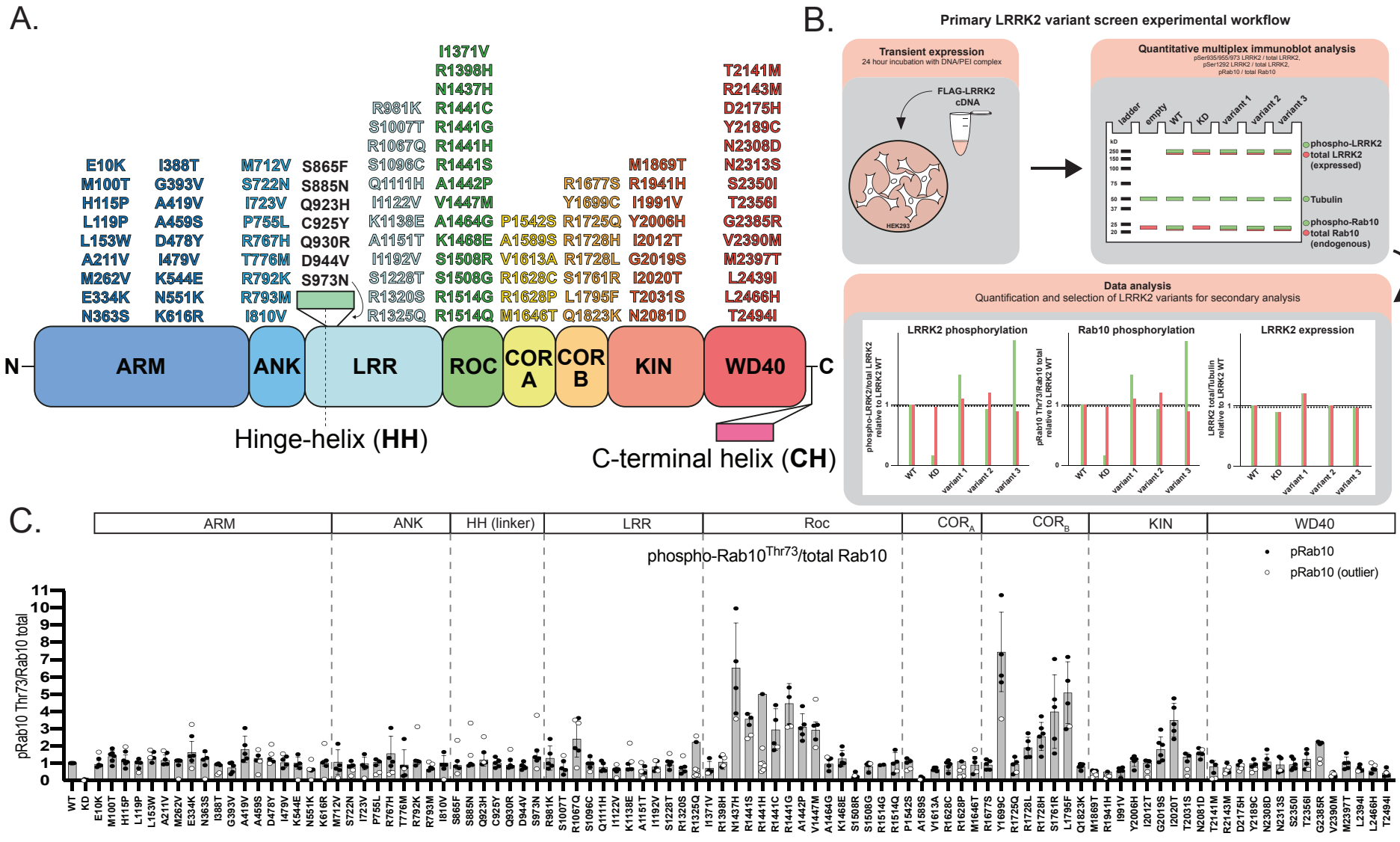

Figure 2

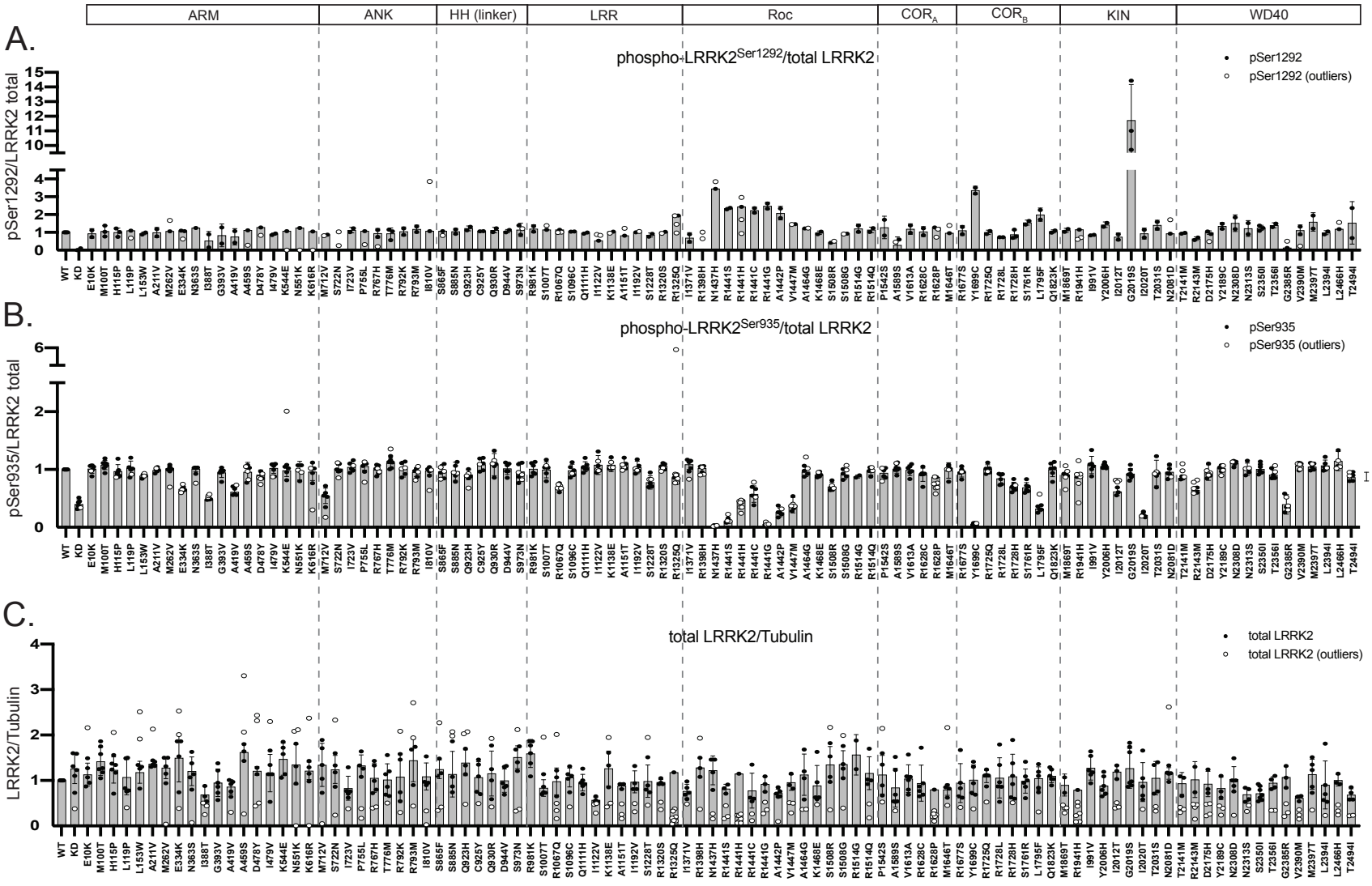

Figure 3

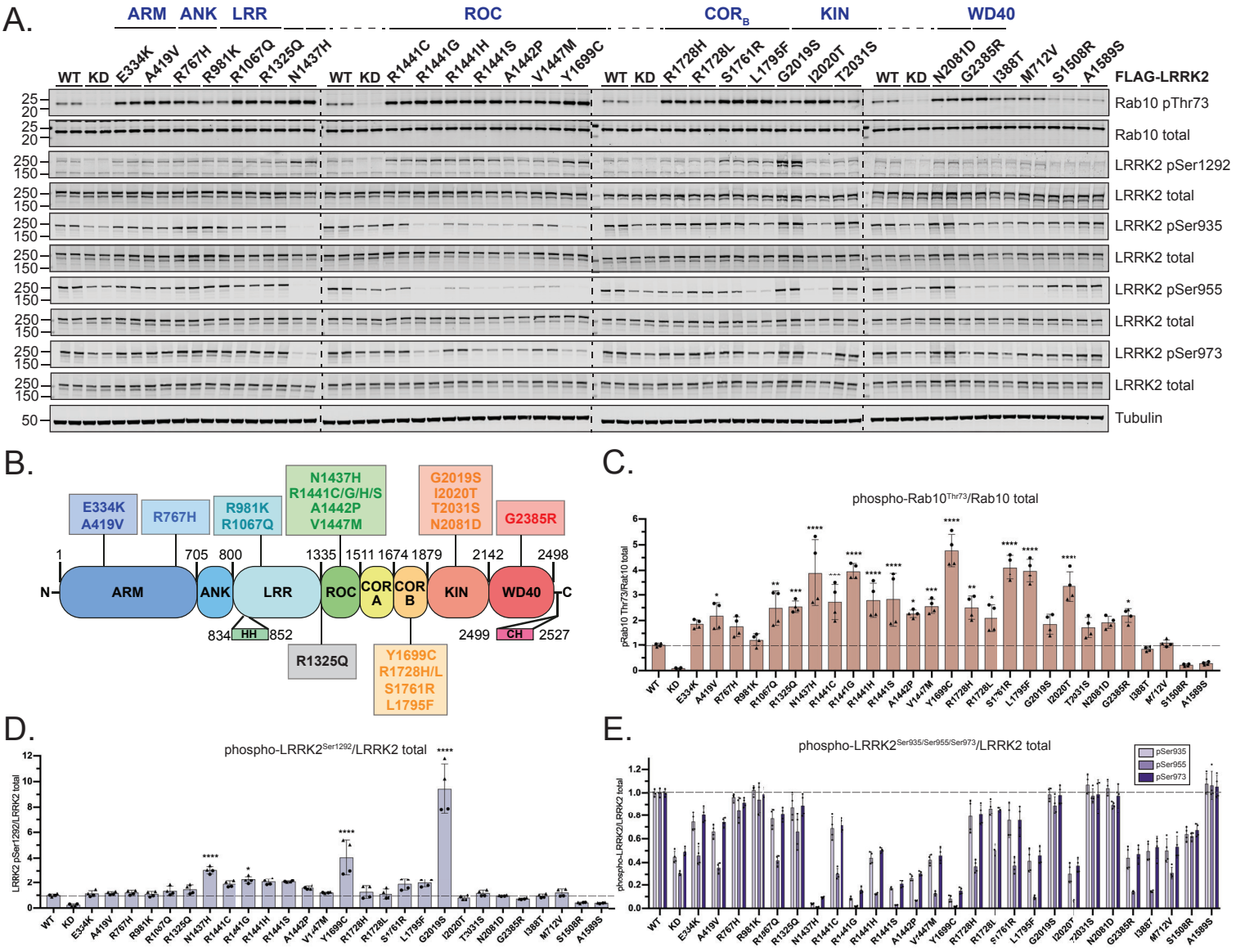

Figure 4

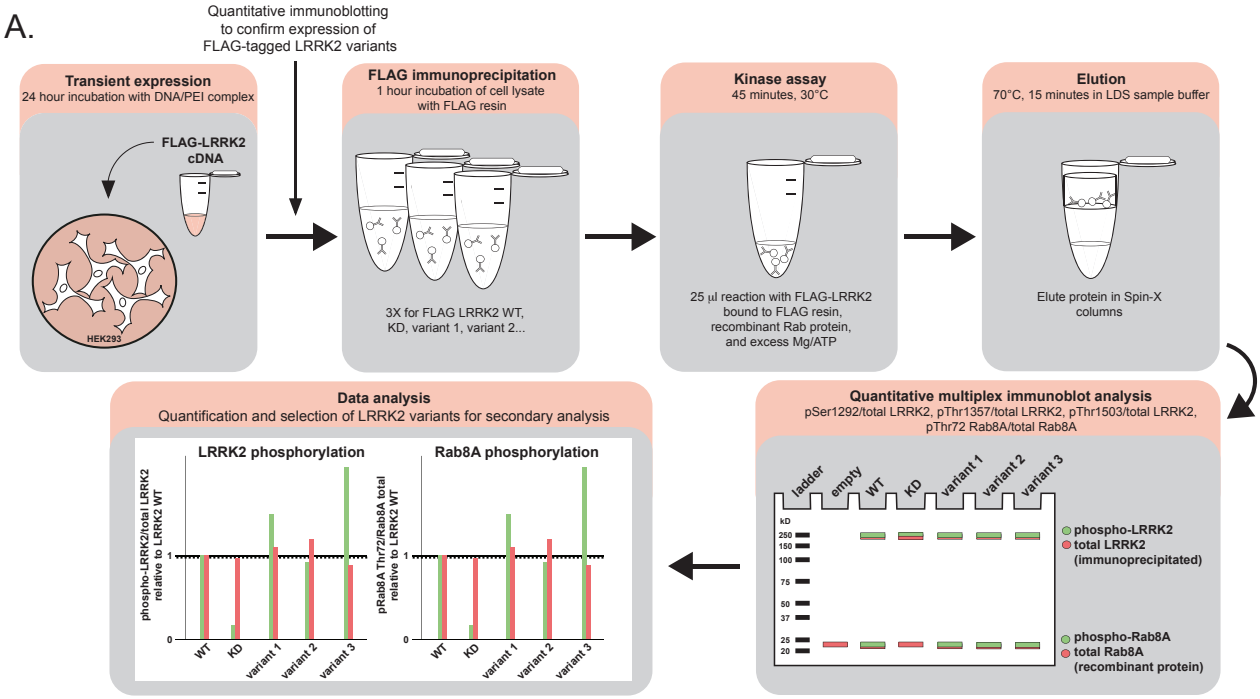

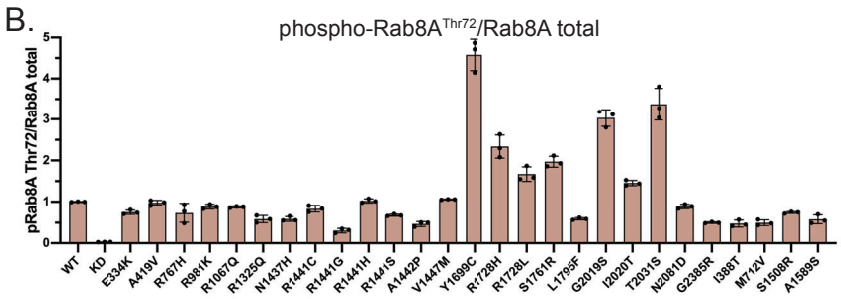

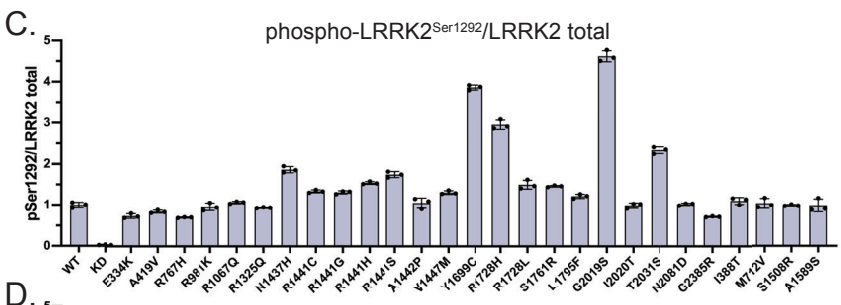

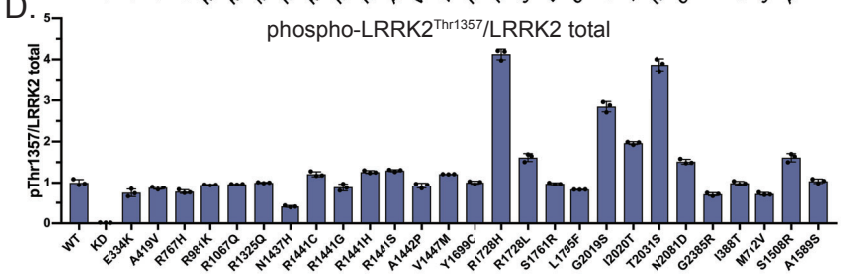

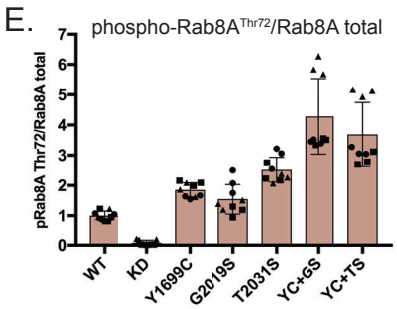

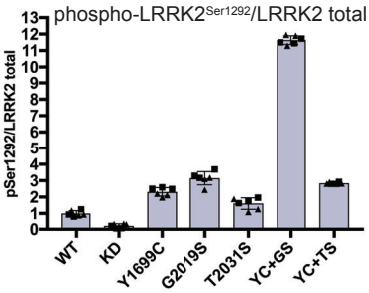

Figure 5

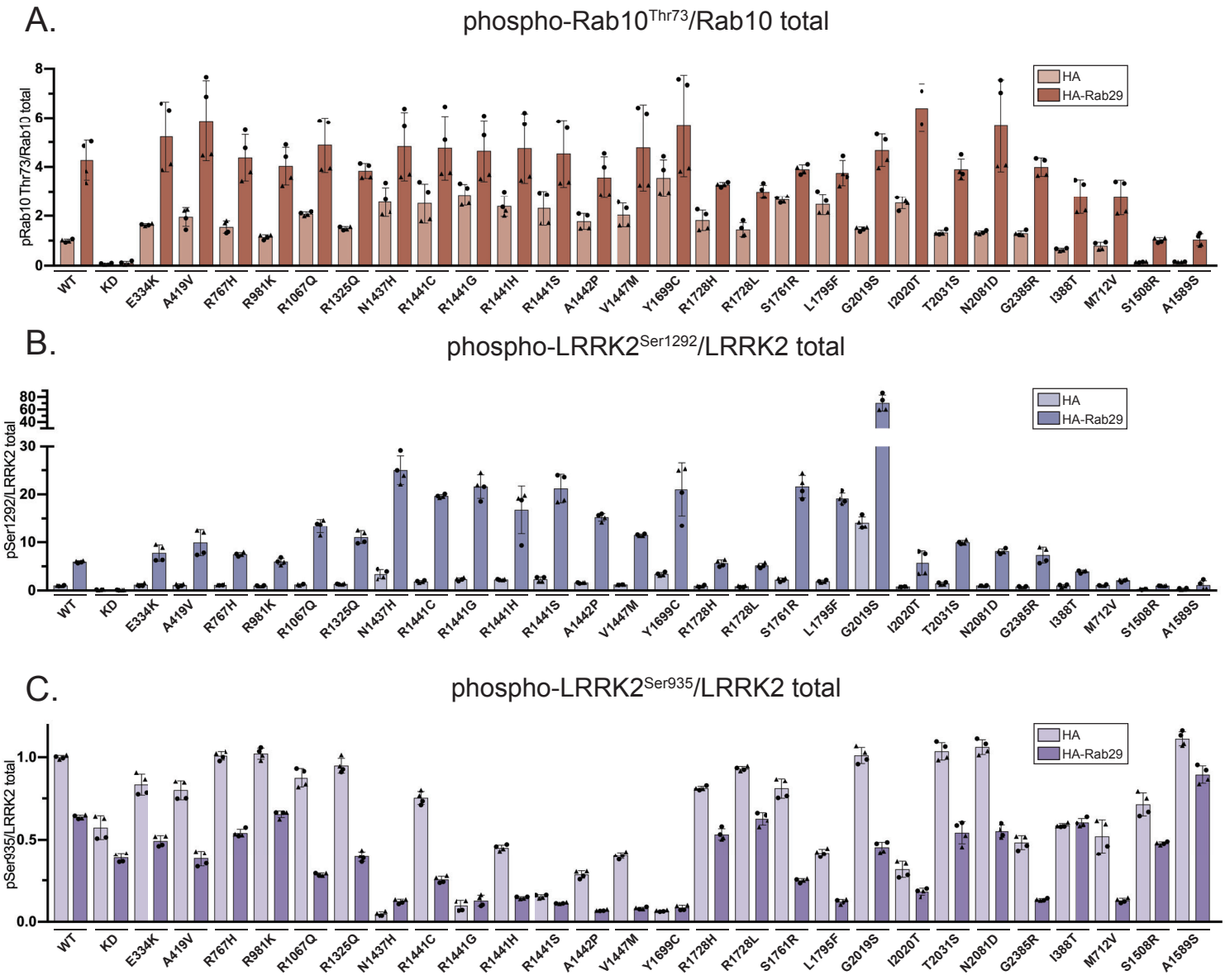

Figure 6

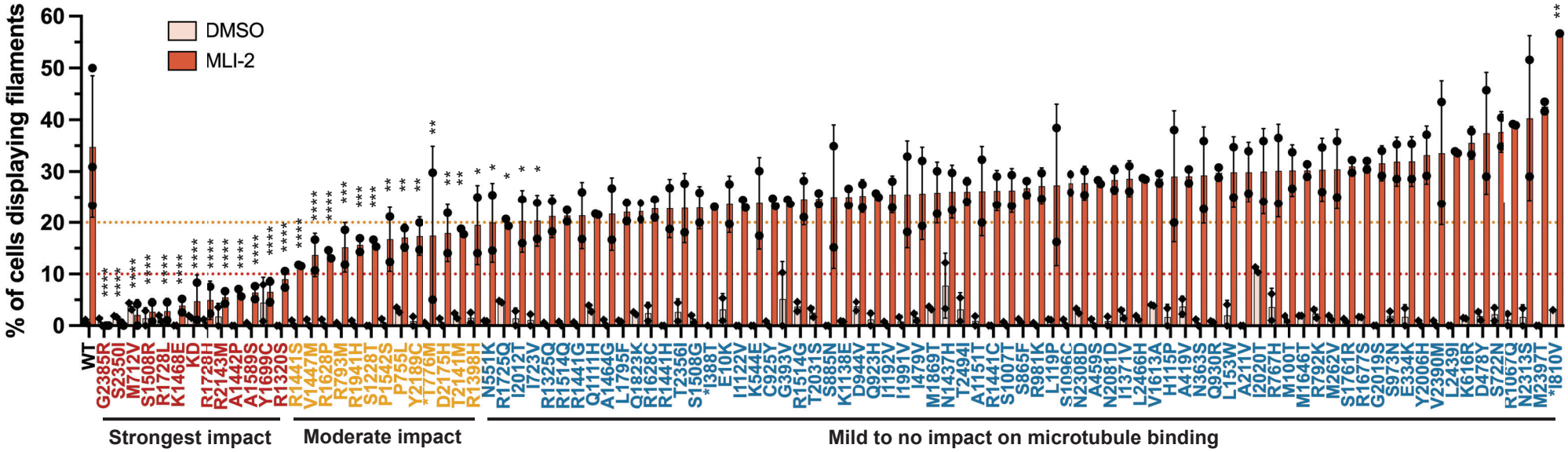

Figure 7

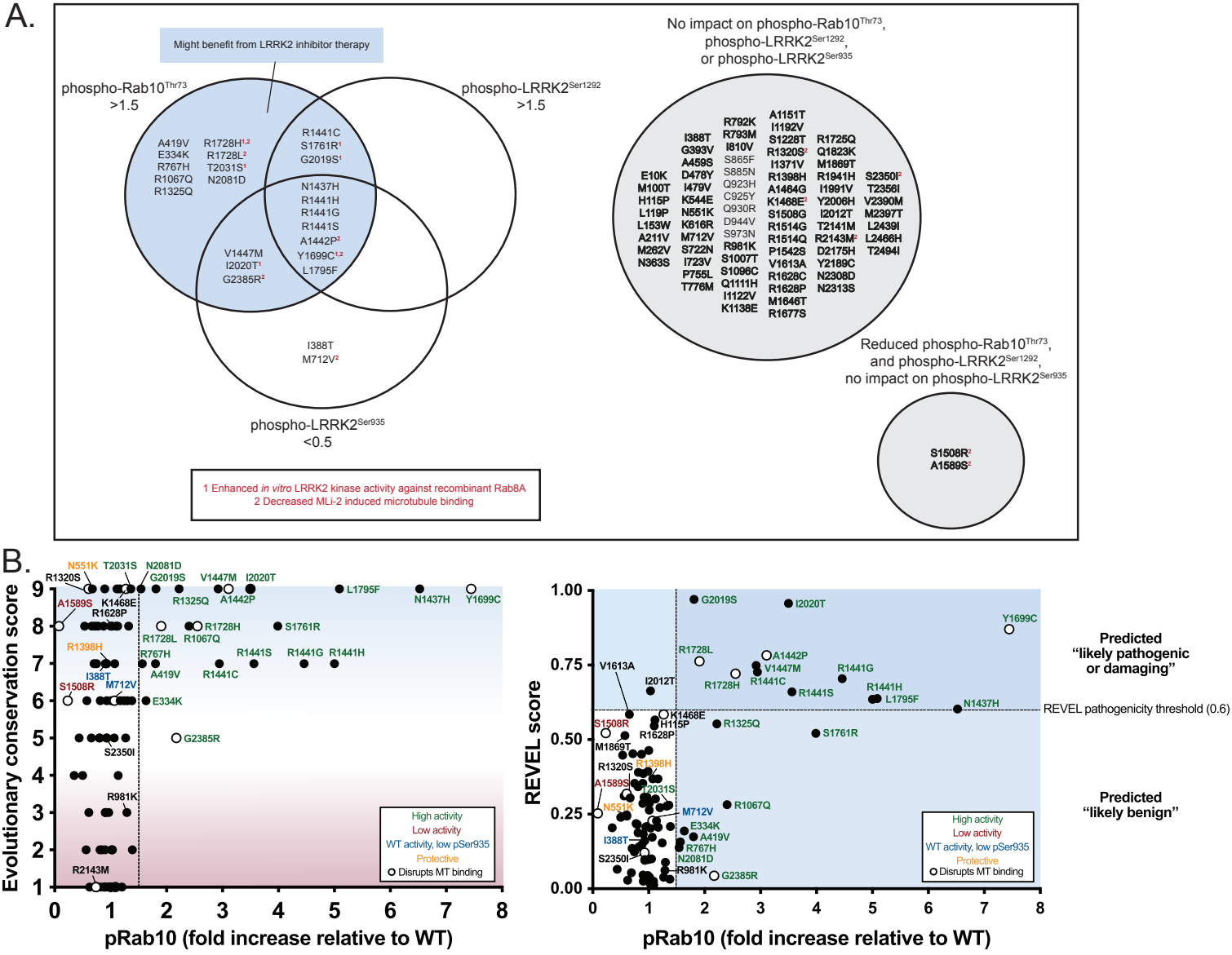

Figure 8

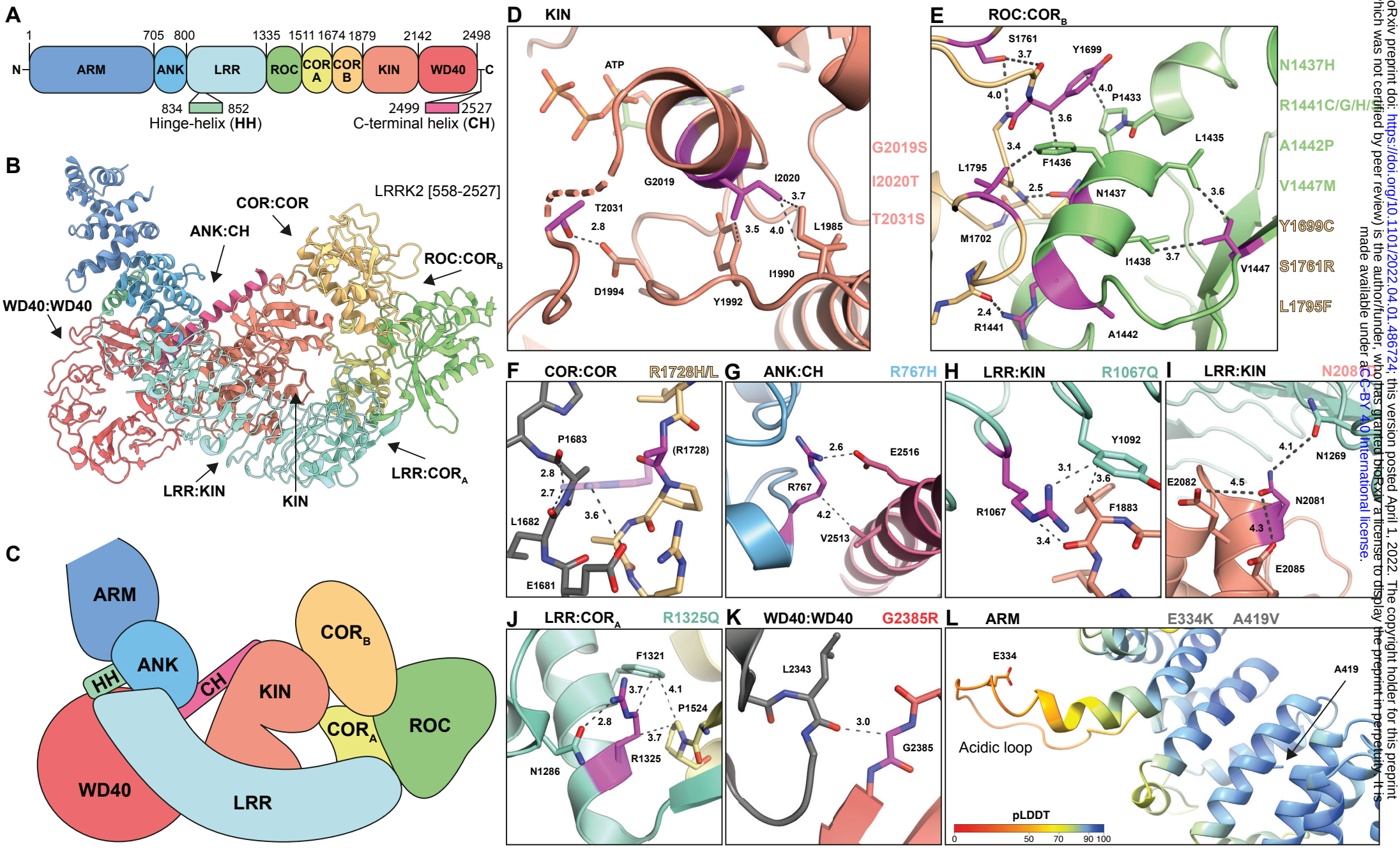

Supplementary Figure 1

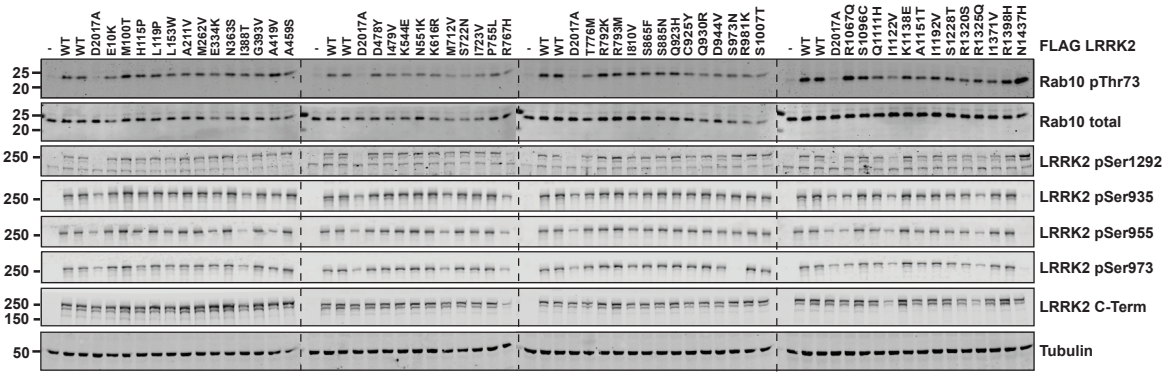

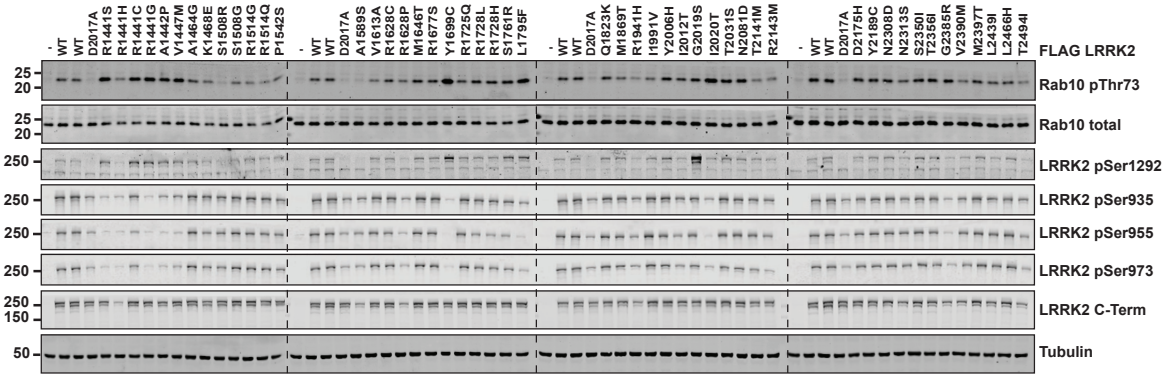

Supplementary Figure 2

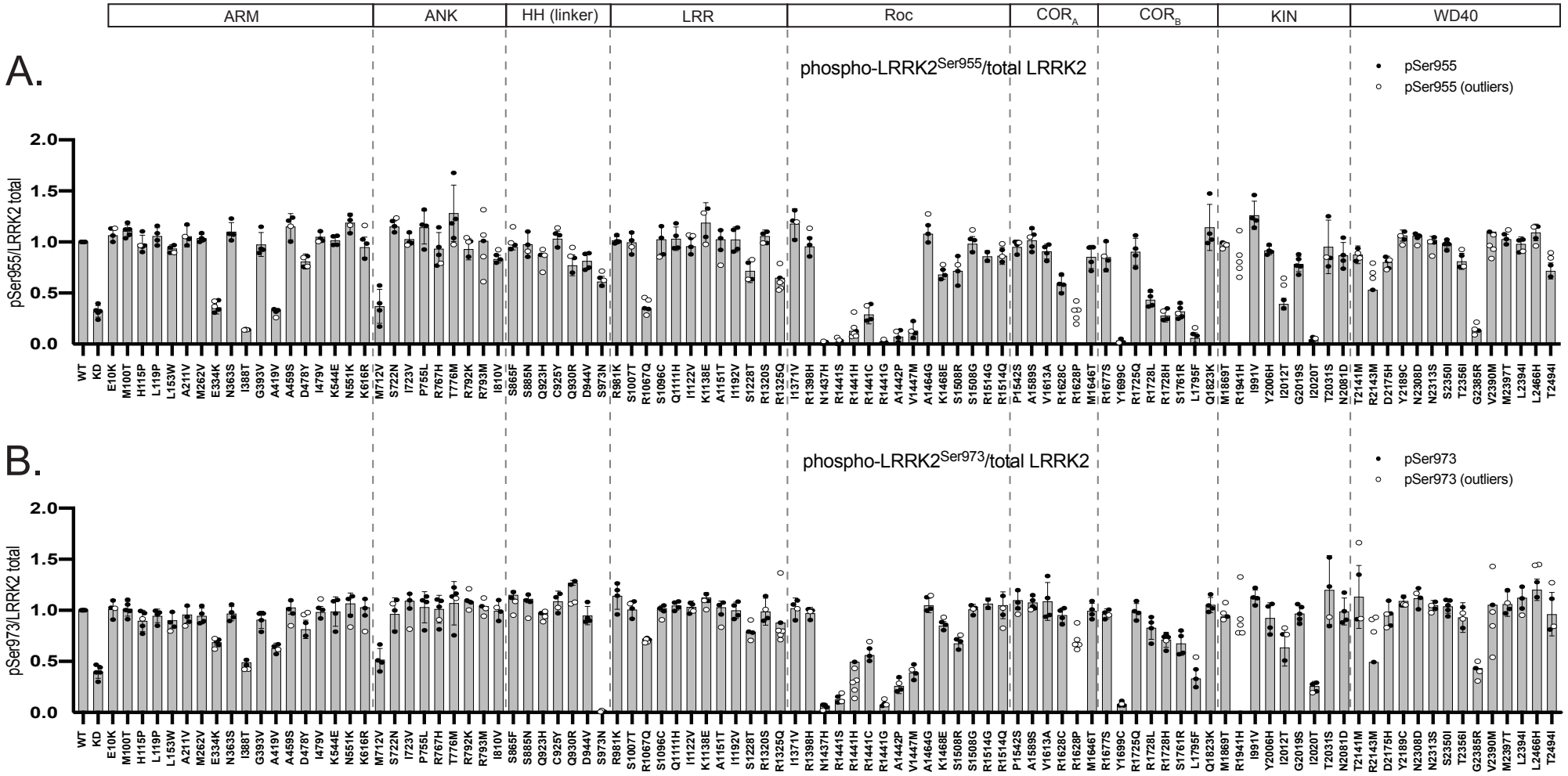

Supplementary Figure 3

A.

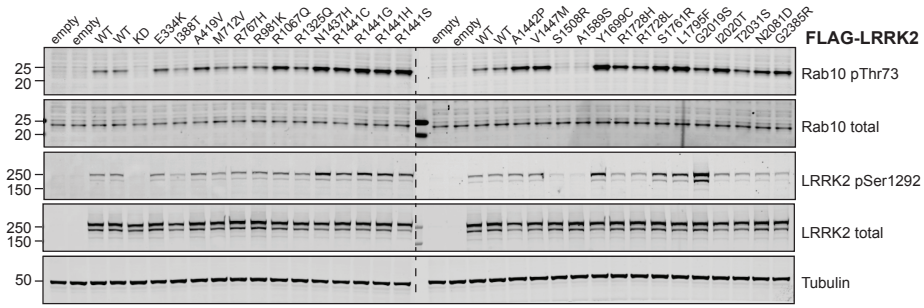

B.

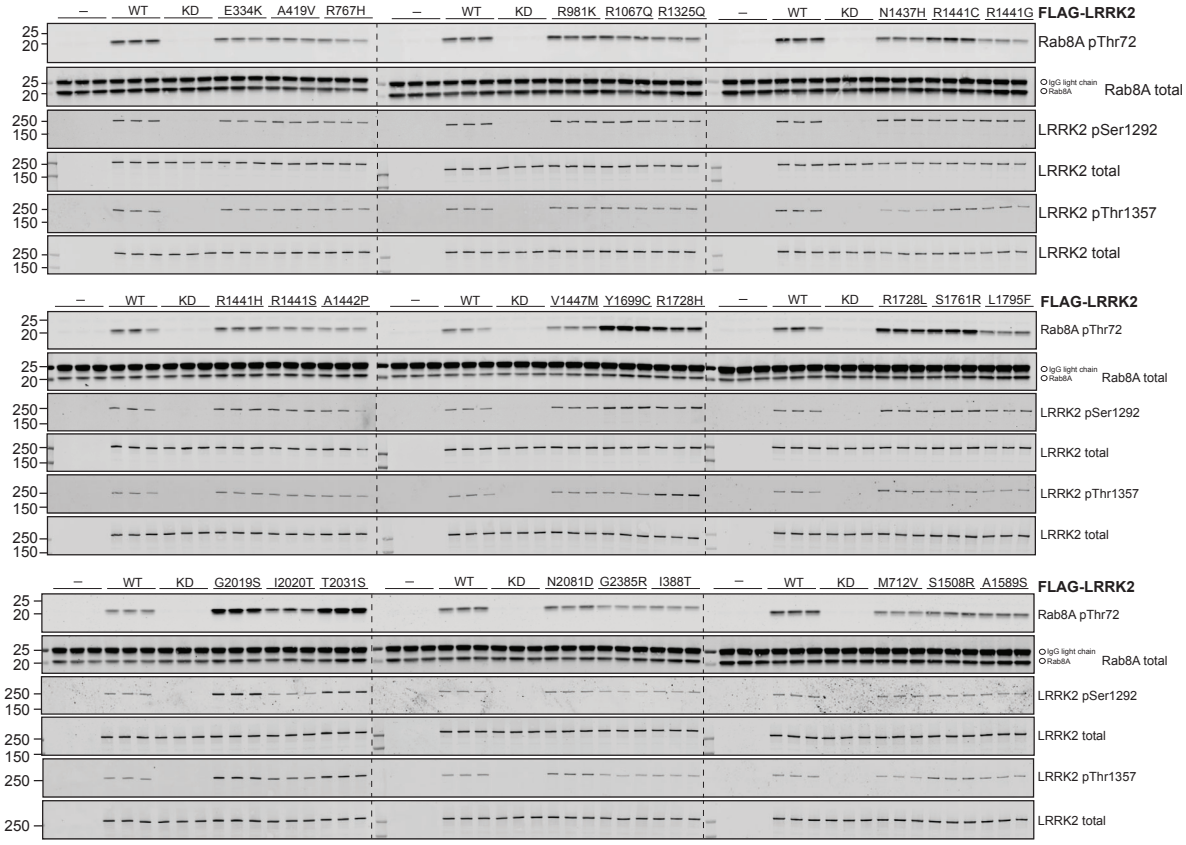

Supplementary Figure 4

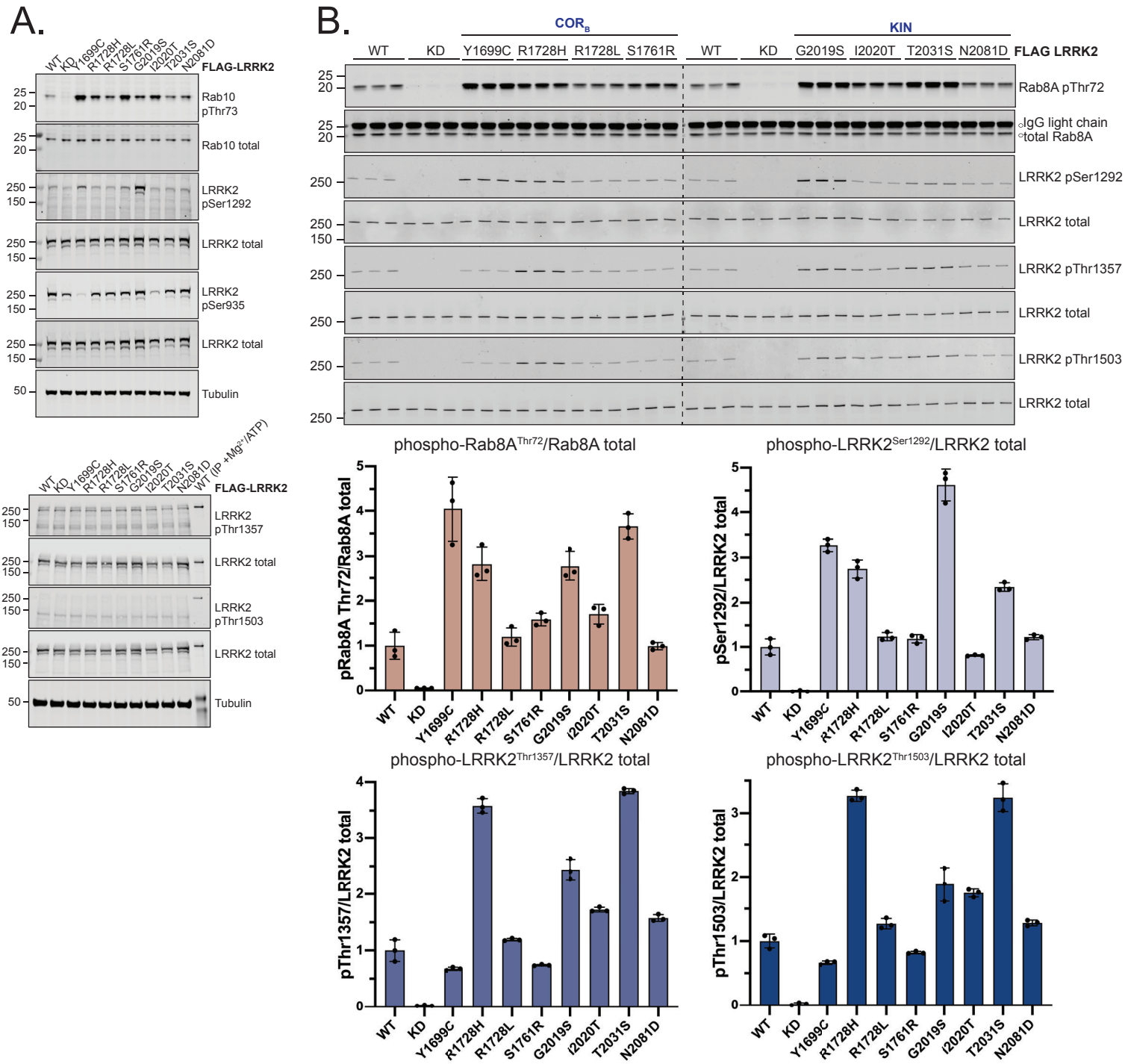

Supplementary Figure 5

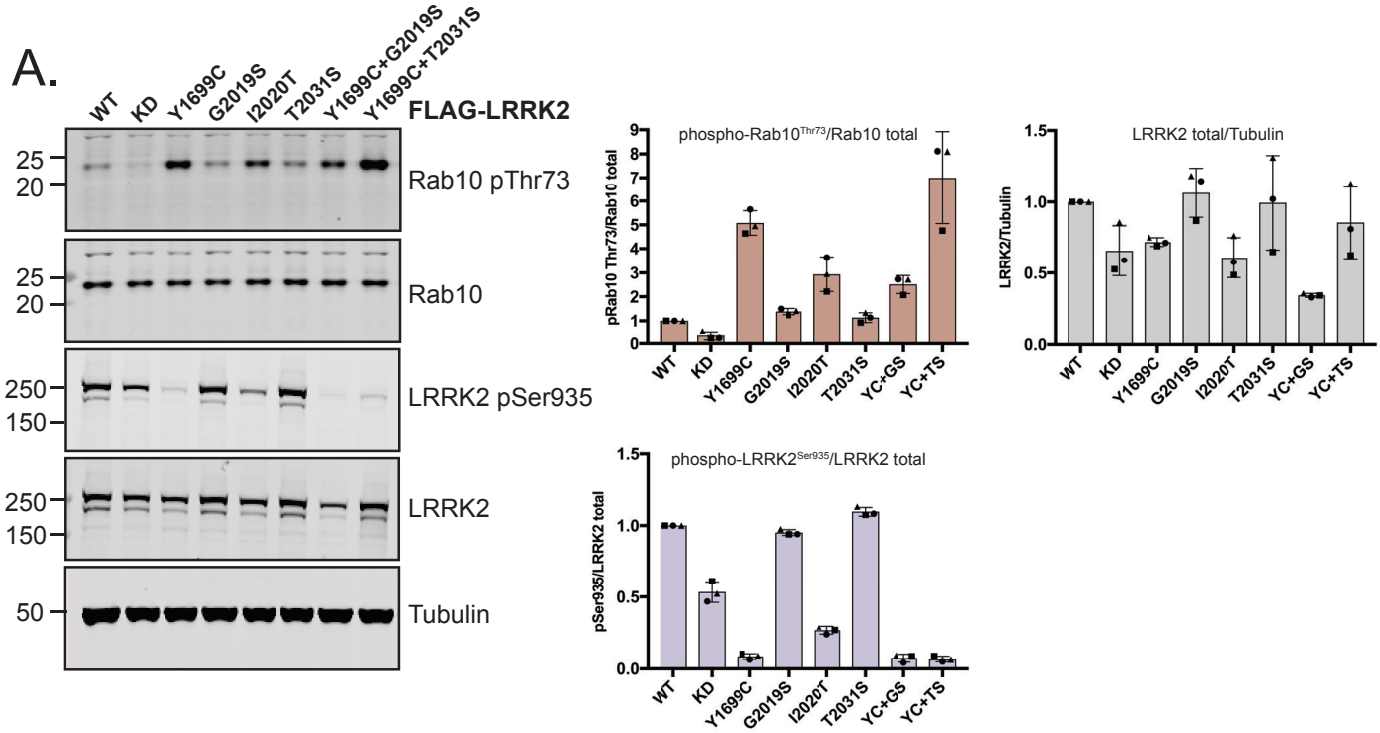

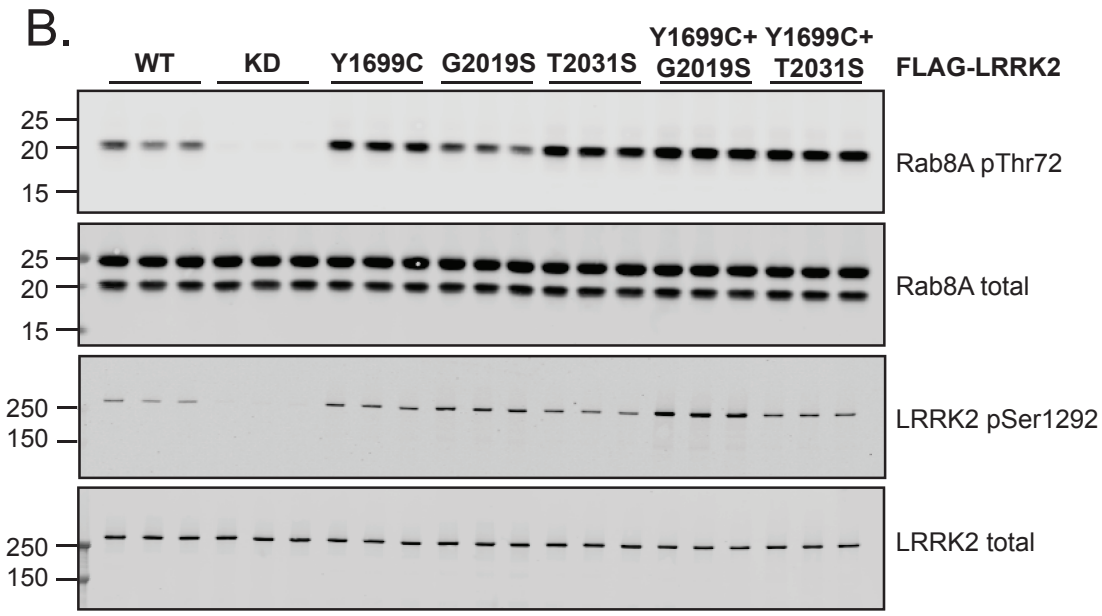

Supplementary Figure 6

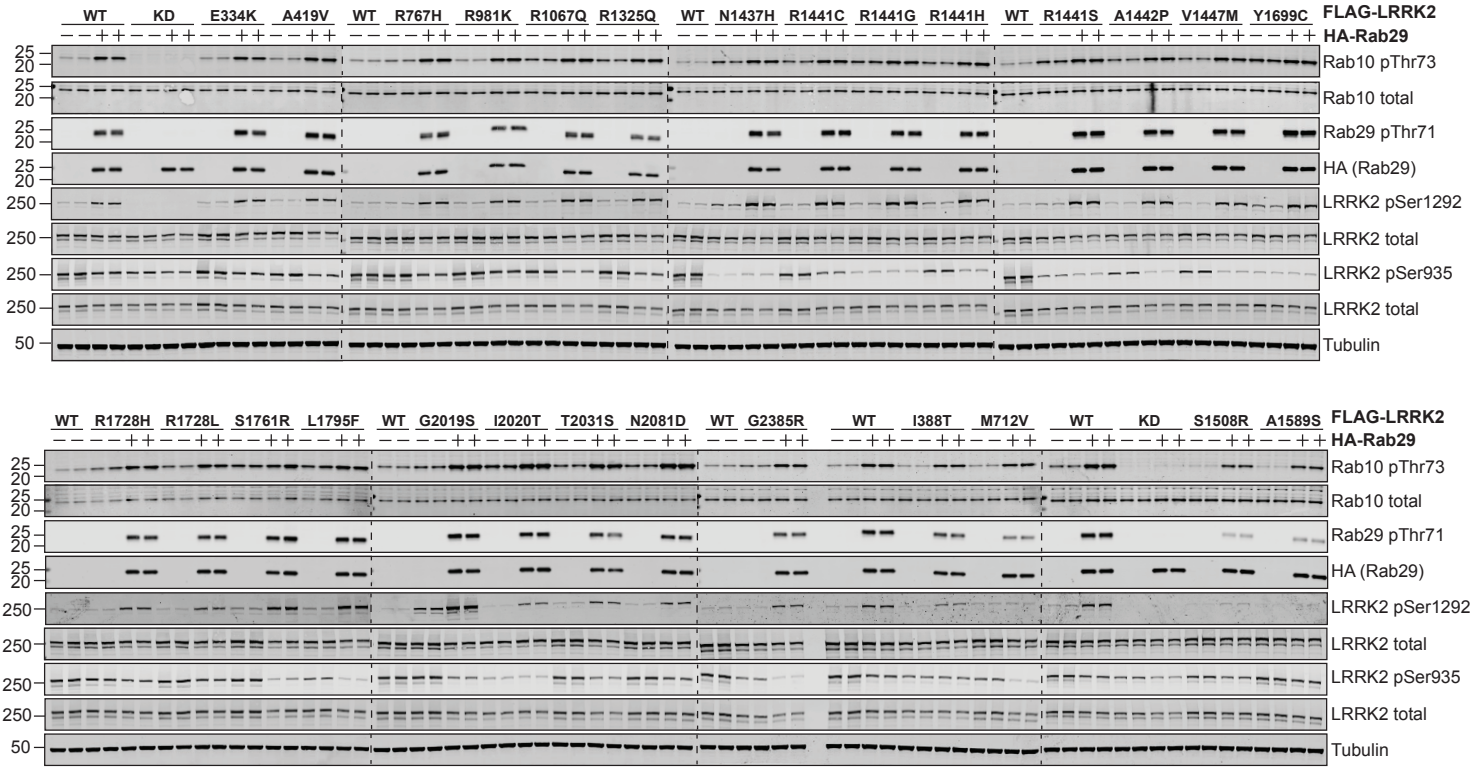

Supplementary Figure 7

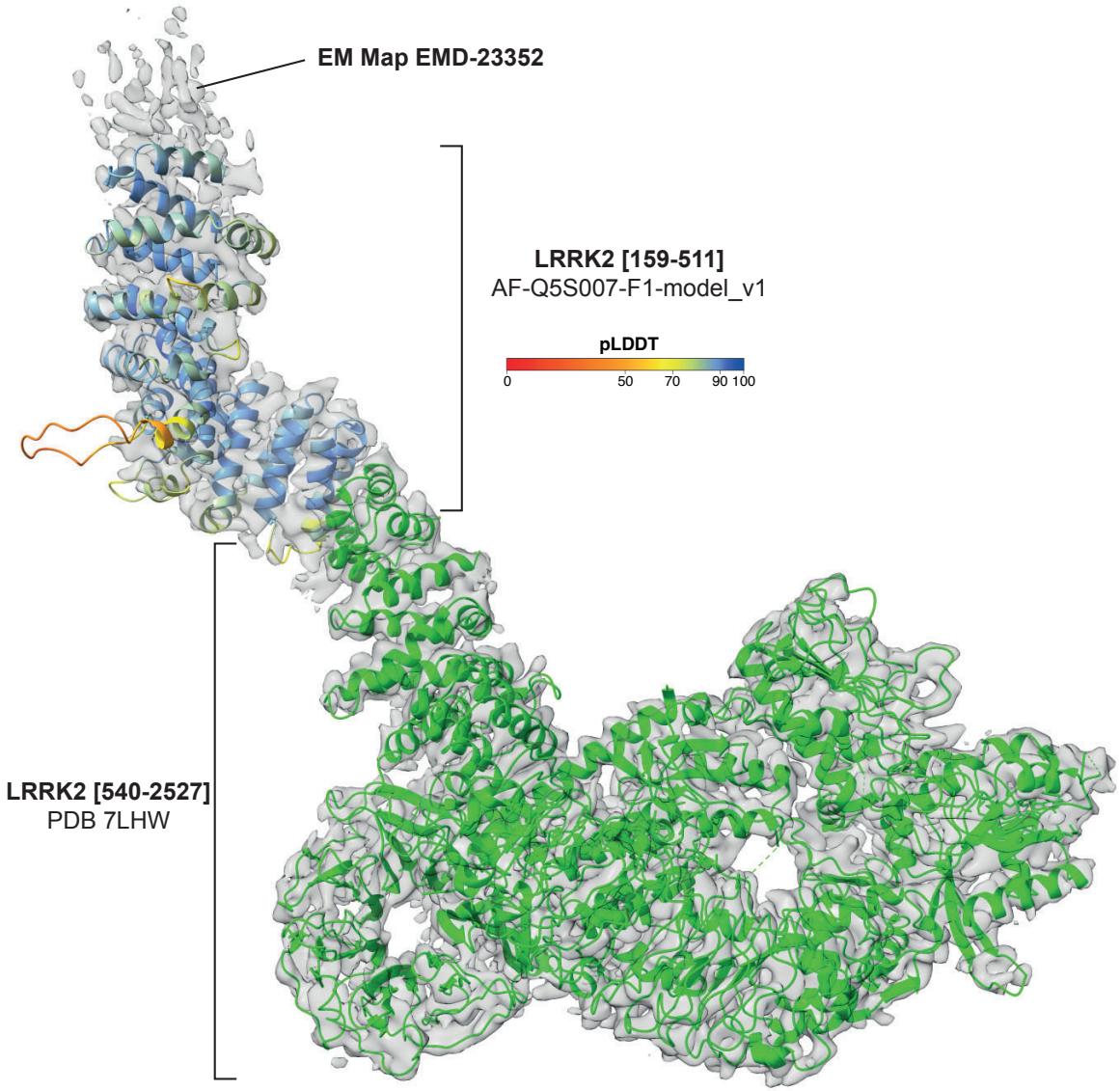

Supplementary Table 1

No.	*Mutation (Single Letter)*	*Mutation*	*Domain location*	*REVEL score*	*Conservation Score*	*Reference*
1	E10K	p.Glu10Lys	ARM	0.207	1	(Nichols *et al.*, 2007)
2	M100T	p.Met100Thr	ARM	0.209	2	(Zhang *et al.*, 2018)
3	H115P	p.His115Pro	ARM	0.566	9	Unpublished*
4	L119P	p.Leu119Pro	ARM	0.464	8	(Ross *et al.*, 2011)*
5	L153W	p.Leu153Trp	ARM	0.277	8	(Zhang *et al.*, 2018)
6	A211V	p.Ala211Val	ARM	0.206	6	(Xiromerisiou *et al.*, 2007)
7	M262V	p.Met262Val	ARM	0.013	1	Unpublished*
8	E334K	p.Glu334Lys	ARM	0.194	6	(Nichols *et al.*, 2007)
9	N363S	p.Asn363Ser	ARM	0.039	5	(Lesage *et al.*, 2009)
10	I388T	p.Ile388Thr	ARM	0.161	7	Unpublished*
11	G393V	p.Gly393Val	ARM	0.124	1	Unpublished*
12	A419V	p.Ala419Val	ARM	0.175	7	(Di Fonzo, Tassorelli, *et al.*, 2006)
13	A459S	p.Ala459Ser	ARM	0.089	6	(Zhang *et al.*, 2018)
14	D478Y	p.Asp478Tyr	ARM	0.369	9	Unpublished*
15	I479V	p.Ile479Val	ARM	0.026	1	Unpublished*
16	K544E	p.Lys544Glu	ARM	0.288	2	(Xiromerisiou *et al.*, 2007)
17	N551K	p.Asn551Lys	ARM	0.248	9	(Di Fonzo, Tassorelli, *et al.*, 2006)*
18	K616R	p.Lys616Arg	ARM	0.264	6	(Wang *et al.*, 2010)
19	M712V	p.Met712Val	ANK	0.228	6	(Paisán-Ruíz *et al.*, 2008)
20	S722N	p.Ser722Asn	ANK	0.098	5	(Zhang *et al.*, 2018)
21	I723V	p.Ile723Val	ANK	0.045	1	(Ross *et al.*, 2011)*
22	P755L	p.Pro755Leu	ANK	0.173	5	(Di Fonzo, Tassorelli, *et al.*, 2006)
23	R767H	p.Arg767His	ANK	0.157	7	(Wu *et al.*, 2013)*
24	T776M	p.Thr776Met	ANK	0.046	1	Unpublished*
25	R792K	p.Arg792Lys	ANK	0.023	1	(Zhang *et al.*, 2018)
26	R793M	p.Arg793Met	ANK	0.305	8	(Berg *et al.*, 2005)
27	I810V	p.Ile810Val	LRR	0.016	2	(Lesage *et al.*, 2009)
28	S865F	p.Ser865Phe	LRR	0.149	1	(Al-Mubarak *et al.*, 2015)*
29	S885N	p.Ser885Asn	LRR	0.025	2	(Wu *et al.*, 2013)
30	Q923H	p.Gln923His	LRR	0.272	1	(Camargos *et al.*, 2010)*
31	C925Y	p.Cys925Tyr	LRR	0.039	1	(Zhang *et al.*, 2018)
32	Q930R	p.Gln930Arg	LRR	0.286	1	(Berg *et al.*, 2005)
33	D944V	p.Asp944Val	LRR	0.14	1	Unpublished*
34	S973N	p.Ser973Asn	LRR	0.032	6	(Haubenberger *et al.*, 2007)
35	R981K	p.Arg981Lys	LRR	0.062	3	(Zhang *et al.*, 2018)
36	S1007T	p.Ser1007Thr	LRR	0.054	2	(Zhang *et al.*, 2018)
37	R1067Q	p.Arg1067Gln	LRR	0.282	8	(Skipper *et al.*, 2005)
38	S1096C	p.Ser1096Cys	LRR	0.204	2	(Berg *et al.*, 2005)

Supplementary Table 1

39	Q1111H	p.Gln1111His	LRR	0.219	8	(Nichols *et al.*, 2007)
40	I1122V	p.Ile1122Val	LRR	0.244	3	(Zimprich *et al.*, 2004)
41	K1138E	p.Lys1138Glu	LRR	0.354	7	Unpublished from Tony Segal
42	A1151T	p.Ala1151Thr	LRR	0.029	1	(Schlitter *et al.*, 2006)
43	I1192V	p.Ile1192Val	LRR	0.215	5	(Nichols *et al.*, 2007)
44	S1228T	p.Ser1228Thr	LRR	0.307	7	(Berg *et al.*, 2005)*
45	R1320S	p.Arg1320Ser	LRR	0.319	9	(Ross *et al.*, 2011)
46	R1325Q	p.Arg1325Gln	LRR	0.553	9	(Nuytemans *et al.*, 2008; Lesage *et al.*, 2009)
47	I1371V	p.Ile1371Val	ROC	0.453	8	(Paisán-Ruíz *et al.*, 2004)
48	R1398H	p.Arg1398His	ROC	0.369	7	(Di Fonzo, Tassorelli, *et al.*, 2006)*
49	N1437H	p.Asn1437His	ROC	0.603	9	(Aasly *et al.*, 2010)
50	R1441S	p.Arg1441Ser	ROC	0.660	7	(Mata *et al.*, 2016)
51	R1441H	p.Arg1441His	ROC	0.635	7	(Mata *et al.*, 2005)
52	R1441C	p.Arg1441Cys	ROC	0.727	7	(Zimprich *et al.*, 2004)
53	R1441G	p.Arg1441Gly	ROC	0.705	7	(Paisán-Ruíz *et al.*, 2004)
54	A1442P	p.Ala1442Pro	ROC	0.783	9	(Huang *et al.*, 2007)
55	V1447M	p.Val1447Met	ROC	0.749	9	(Zhang *et al.*, 2018)
56	A1464G	p.Ala1464Gly	ROC	0.209	3	(Yonova-Doing *et al.*, 2012)
57	K1468E	p.Lys1468Glu	ROC	0.585	9	(Nuytemans *et al.*, 2008)*
58	S1508R	p.Ser1508Arg	ROC	0.522	6	Unpublished- online PhD presentation (2009)
59	S1508G	p.Ser1508Gly	ROC	0.390	6	(Janković *et al.*, 2015)
60	R1514G	p.Arg1514Gly	COR_A	0.354	9	Unpublished
61	R1514Q	p.Arg1514Gln	COR_A	0.1	9	(Mata *et al.*, 2005; Nichols *et al.*, 2007; Toft *et al.*, 2007)*
62	P1542S	p.Pro1542Ser	COR_A	0.228	4	(Mata *et al.*, 2005)*
63	A1589S	p.Ala1589Ser	COR_A	0.253	8	Unpublished*
64	V1613A	p.Val1613Ala	COR_A	0.585	5	(Pchelina *et al.*, 2008)
65	R1628C	p.Arg1628Cys	COR_A	0.451	8	(Bryant *et al.*, 2021)
66	R1628P	p.Arg1628Pro	COR_A	0.546	8	(Mata *et al.*, 2005)*
67	M1646T	p.Met1646Thr	COR_A	0.184	3	(Mata *et al.*, 2005)*
68	R1677S	p.Arg1677Ser	COR_B	0.386	7	(Zhang *et al.*, 2018)
69	Y1699C	p.Tyr1699Cys	COR_B	0.87	9	(Zimprich *et al.*, 2004)
70	R1725Q	p.Arg1725Gln	COR_B	0.095	6	(Shojaee *et al.*, 2009)
71	R1728L	p.Arg1728Leu	COR_B	0.763	8	(Paisán-Ruíz *et al.*, 2008)
72	R1728H	p.Arg1728His	COR_B	0.721	8	(Paisán-Ruíz *et al.*, 2008)
73	S1761R	p.Ser1761Arg	COR_B	0.521	8	(Lorenzo-Betancour *et al.*, 2012)
74	L1795F	p.Leu1795Phe	COR_B	0.638	9	(Nichols *et al.*, 2007)
75	Q1823K	p.Gln1823Lys	COR_B	0.188	2	(Shojaee *et al.*, 2009)
76	M1869T	p.Met1869Thr	COR_B	0.514	6	(Mata *et al.*, 2005)
77	R1941H	p.Arg1941His	KIN	0.24	4	(Khan *et al.*, 2005)*

Supplementary Table 1

78	I1991V	p.Ile1991Val	KIN	0.448	8	(Janković *et al.*, 2015)
79	Y2006H	p.Tyr2006His	KIN	0.301	8	(Lesage *et al.*, 2007)
80	I2012T	p.Ile2012Thr	KIN	0.664	8	(Lu *et al.*, 2005)
81	G2019S	p.Gly2019Ser	KIN	0.97	9	(Di Fonzo *et al.*, 2005; Gilks *et al.*, 2005; Nichols *et al.*, 2005)*
82	I2020T	p.Ile2020Thr	KIN	0.957	9	(Zimprich *et al.*, 2004; Funayama *et al.*, 2005)
83	T2031S	p.Thr2031Ser	KIN	0.280	9	(Lesage *et al.*, 2007)
84	N2081D	p.Asn2081Asp	KIN	0.138	9	(Ross *et al.*, 2011)*
85	T2141M	p.Thr2141Met	KIN	0.342	5	(Paisán-Ruíz *et al.*, 2008)
86	R2143M	p.Arg2143Met	WD40	N/A	1	(Nichols *et al.*, 2010)**
87	D2175H	p.Asp2175His	WD40	0.307	1	(Shojaee *et al.*, 2009)
88	Y2189C	p.Tyr2189Cys	WD40	0.394	1	(Nuytemans *et al.*, 2008)
89	N2308D	p.Asn2308Asp	WD40	0.025	1	(Zhang *et al.*, 2018)
90	N2313S	p.Asn2313Ser	WD40	0.043	3	(Zhang *et al.*, 2018)
91	S2350I	p.Ser2350Ile	WD40	0.121	5	(Zhang *et al.*, 2018)
92	T2356I	p.Thr2356Ile	WD40	0.154	6	(Khan *et al.*, 2005)
93	G2385R	p.Gly2385Arg	WD40	0.044	5	(Mata *et al.*, 2005; Di Fonzo, Wu-Chou, *et al.*, 2006) *
94	V2390M	p.Val2390Met	WD40	0.205	4	(Clarimón *et al.*, 2008)
95	M2397T	p.Met2397Thr	WD40	0.098	1	(Di Fonzo, Tassorelli, *et al.*, 2006)*
96	L2439I	p.Leu2439Ile	WD40	0.135	7	(Shojaee *et al.*, 2009)
97	L2466H	p.Leu2466His	WD40	0.311	2	(Paisán-Ruíz *et al.*, 2008)
98	T2494I	p.Thr2494Ile	WD40	0.065	5	(Kessler *et al.*, 2018)

*LRRK2 variants disclosed by Michael J Fox Foundation through Parkinson's Progression Markers Initiative (PPMI) clinical database

**R2143M is not associated with any previously reported patient data. R2143H was previously reported in (Paisán-Ruíz *et al.*, 2008)